NASA TECHNICAL NOTE

NASA TN D-7499

NASA TN D-7499

RELAXATION OF AN UNSTEADY TURBULENT BOUNDARY LAYER ON A FLAT PLATE IN AN EXPANSION TUBE

by Roop N. Gupta and Robert L. Trimpi

Langley Research Center

Hampton, Va. 23665

NATIONAL AERONAUTICS AND SPACE ADMINISTRATION • WASHINGTON, D. C. • JUNE 1974

1. Report No.	2. Government Accession No.	3. Recipient's Catalog No.
NASA TN D-7499		

4. Title and Subtitle	5. Report Date
RELAXATION OF AN UNSTEADY TURBULENT BOUNDARY LAYER ON A FLAT PLATE IN AN EXPANSION TUBE	June 1974
	6. Performing Organization Code

7. Author(s)	8. Performing Organization Report No.
Roop N. Gupta and Robert L. Trimpi	L-9168
	10. Work Unit No.
	502-07-01-02

9. Performing Organization Name and Address	11. Contract or Grant No.
NASA Langley Research Center Hampton, Va. 23665	
	13. Type of Report and Period Covered
	Technical Note

12. Sponsoring Agency Name and Address	14. Sponsoring Agency Code
National Aeronautics and Space Administration Washington, D.C. 20546	

15. Supplementary Notes

16. Abstract

An analysis is presented for the relaxation of a turbulent boundary layer on a semi-infinite flat plate after passage of a shock wave and a trailing driver gas-driven gas interface. The problem has special application to expansion-tube flows. The flow-governing equations have been transformed into the Crocco variables, and a time-similar solution is presented in terms of the dimensionless distance-time variable α and the dimensionless velocity variable β. An eddy-viscosity model, similar to that of time-steady boundary layers, is applied to the inner and outer regions of the boundary layer. A turbulent Prandtl number equal to the molecular Prandtl number is used to relate the turbulent heat flux to the eddy viscosity. The numerical results, obtained by using the Gauss-Seidel line-relaxation method, indicate that a fully turbulent boundary layer relaxes faster to the final steady-state values of heat transfer and skin friction than a laminar boundary layer. The results also give a fairly good estimate of the local skin friction and heat transfer for near steady-flow conditions.

17. Key Words (Suggested by Author(s))	18. Distribution Statement
Unsteady turbulent boundary layers on flat plates Eddy-viscosity treatment Expansion-tube flow Numerical solution of singular parabolic equations	Unclassified – Unlimited STAR Category 12

19. Security Classif. (of this report)	20. Security Classif. (of this page)	21. No. of Pages	22. Price*
Unclassified	Unclassified	56	$3.75

*For sale by the National Technical Information Service, Springfield, Virginia 22151

RELAXATION OF AN UNSTEADY TURBULENT BOUNDARY LAYER ON A FLAT PLATE IN AN EXPANSION TUBE

By Roop N. Gupta and Robert L. Trimpi
Langley Research Center

SUMMARY

An analysis is presented for the relaxation of a turbulent boundary layer on a semi-infinite flat plate after passage of a shock wave and a trailing driver gas-driven gas interface. The problem has special application to expansion-tube flows. The flow-governing equations have been transformed into the Crocco variables, and a time-similar solution is presented in terms of the dimensionless distance-time variable α and the dimensionless velocity variable β. An eddy-viscosity model, similar to that of time-steady boundary layers, is applied to the inner and outer regions of the boundary layer. A turbulent Prandtl number equal to the molecular Prandtl number is used to relate the turbulent heat flux to the eddy viscosity. The numerical results, obtained by using the Gauss-Seidel line-relaxation method, indicate that a fully turbulent boundary layer relaxes faster to the final steady-state values of heat transfer and skin friction than a laminar boundary layer. The results also give a fairly good estimate of the local skin friction and heat transfer for near steady-flow conditions.

INTRODUCTION

When an unsteady flow occurs in the vicinity of a body, there is a time lag during which the flow characteristics adjust toward the new situation. This time lag results from different mechanisms in the external flow field and the boundary layer. The external flow field may have a quasi-steady character after a time required by the fluid particles to travel a few body lengths. This relaxation of the flow field is the result of wave-propagation mechanisms. The boundary-layer flow adjustment, however, is the result of molecular or turbulent diffusion, which is a much slower process than wave propagation.

In an expansion tube (ref. 1) the interest lies in simulating the steady flow past a model. The distance-time plot of expansion-tube flow cycle is shown in figure 1. As pointed out earlier, the diffusion processes require time, yet the quasi-steady flow available in the test facility exists for only a short time. It therefore becomes essential to ascertain that the establishment of the boundary layer (on the model) takes place in a time which is substantially less than the available test time. This situation is an asymp-

totic one in which the departure from the final state is vanishingly small after a certain period of time.

In references 2 and 3 results have been obtained for the establishment of a laminar boundary layer on a test model in an expansion tube. It is shown therein that an all-nitrogen time-dependent boundary layer on a flat plate relaxes to the Blasius value in about three-tenths of the distance (measured from the leading edge) traversed by the interface in the free stream. In practice, the boundary layer may not remain laminar. Under such circumstances it is of interest to know how the laminar results of references 2 and 3 are modified if the boundary layer is assumed fully turbulent from the beginning of its formation. In this study an analysis is presented for the wave-induced fully developed turbulent compressible boundary layer (in region 5, fig. 1) over a semi-infinite flat plate in an expansion tube. The time and distance required to complete transition from laminar to turbulent flow are not considered herein. For quantitative evaluation of the boundary-layer properties, nitrogen has been used both in the test as well as in the acceleration gas region. The turbulent boundary layer is regarded as a composite layer consisting of inner and outer regions with separate eddy-viscosity expression for each region (in a manner similar to that employed for time-steady turbulent boundary-layer problems; see ref. 4, for example). The turbulent Prandtl number is assumed equal to the molecular Prandtl number and is used to relate the turbulent eddy conductivity to the eddy viscosity. The governing equations are treated in the Crocco transformed plane, and the conically self-similar solutions have been obtained by using the Gauss-Seidel line-relaxation method similar to the one employed in reference 2.

SYMBOLS

A ratio of shock velocity to free-stream velocity, U_S/U_O

a fraction of model length

$C = \frac{\mu\rho}{(\mu\rho)_W}$

c_f local skin-friction coefficient, $\frac{\tau_W}{\frac{1}{2}\left(\rho_W U_O^2\right)}$

c_p specific heat at constant pressure

c_v specific heat at constant volume

G	Blasius shear function, $\phi(0,\beta)$
H	dimensionless enthalpy difference
H_G	Blasius enthalpy function, $H(0,\beta)$
H_M	Mirels enthalpy function, $H(1,\beta)$
H_o	dimensionless enthalpy difference behind shock in free stream, $\frac{h_o - h_w}{h_w}$
h	local enthalpy; also, step size in numerical method
h_o	local enthalpy behind shock in free stream
K_1	constant in eddy-viscosity model (eq. 40), 0.4
K_2	constant in eddy-viscosity model (eq. 41), 0.0168
k	thermal conductivity
k_T	eddy conductivity
L	reference length
M	Mirels shear function, $\phi(1,\beta)$
M_s	shock Mach number
M_∞	free-stream Mach number
N_{Pr}	molecular Prandtl number, $\frac{c_p\mu}{k}$
$N_{Pr,t}$	turbulent Prandtl number, $\frac{c_p\epsilon}{k_T}$
N_{St}	Stanton number, $\frac{-q_w}{\rho_w U_o c_p (T_r - T_w)}$

n reciprocal of velocity exponent in boundary layer, $\frac{u}{U_o} = \left(\frac{y}{\delta}\right)^{1/n}$

p pressure; also, iteration parameter

q heat-transfer rate

R gas constant

$R_{e,x}$ Reynolds number based on free-stream conditions, $\rho_e U_o x / \mu_e$

$R_{w,L}$ Reynolds number based on L, $\rho_w U_o L / \mu_w$

$R_{w,x}$ Reynolds number based on x, $\rho_w U_o x / \mu_w$

$R_{\infty,x} = \frac{\rho_\infty U_o x}{\mu_\infty}$

T temperature, K

T_o free-stream temperature in region between shock and interface

T_r recovery temperature

T_{st} stagnation temperature in free stream (having temperature T_∞)

T_∞ free-stream temperature in region between interface and expansion fan

t time, measured so that at $t = 0$ shock wave is located at leading edge of plate

t^* time, measured so that at $t^* = 0$ interface is located at leading edge of plate

U_e free-stream velocity in shock-fixed coordinate system

U_o free-stream velocity

U_s shock velocity

U_w plate velocity in shock-fixed coordinate system

u velocity component parallel to plate surface in boundary layer

v velocity component normal to plate surface in boundary layer

$\tilde{v} = v + \dfrac{\overline{\rho' v'}}{\rho}$

x distance from leading edge along plate in x,t coordinate system fixed to plate

$x_s = U_s t$

x^* distance from leading edge along plate in x^*,t^* coordinate system fixed to plate

x^+ distance from foot of shock in shock-fixed x^+,y^+ coordinate system

y normal distance from plate

y_m location separating inner and outer regions of turbulent boundary layer

y^+ normal distance from plate in shock-fixed x^+,y^+ coordinate system

α conical coordinate in MR limit, $x/U_o t$

α^* conical coordinate in BL limit, $x^*/U_o t^*$

β dimensionless velocity, u/U_o

$\tilde{\beta} = \dfrac{U_w}{U_e} + \dfrac{U_e - U_w}{U_e}\beta$

γ ratio of specific heats

$\bar{\gamma}$ dimensionless time in MR limit, $\rho_w U_o^2 t/\mu_w$

$\overline{\gamma}^*$ dimensionless time in BL limit, $\rho_w U_o^2 t^* / \mu_w$

δ thickness of velocity boundary layer

δ^*_{inc} incompressible boundary-layer displacement thickness, $\int_0^\infty \left(1 - \frac{u}{U_o}\right) dy$

ϵ eddy viscosity

$\bar{\epsilon} = 1 + \frac{\epsilon}{\mu}$

$\bar{\bar{\epsilon}} = \frac{\bar{\epsilon}}{\left(R_{w,x}\right)^{3/5}}$

$\hat{\epsilon} = 1 + \frac{\epsilon}{\mu} \frac{N_{Pr}}{N_{Pr,t}} = 1 + \frac{k_T}{k}$

η dimensionless y-coordinate

θ_{inc} incompressible boundary-layer momentum thickness, $\int_0^\infty \frac{u}{U_o}\left(1 - \frac{u}{U_o}\right) dy$

μ dynamic viscosity

ν kinematic viscosity

ρ density

τ shear stress

ϕ shear function defined by equation (23a)

$\overline{\phi}$ dimensionless shear stress defined by equation (20a)

Subscripts:

e edge of boundary layer

I instantaneous value

i inner region of turbulent boundary layer

m count of steps in α-direction

max maximum

n count of steps in β-direction

o outer region of turbulent boundary layer

t total condition

w evaluated at wall

∞ free stream

Superscripts:

' fluctuating component

+ quantities in shock-fixed coordinate system

Abbreviations:

BL Blasius

MR Mirels

N_2 nitrogen

BACKGROUND

There does not appear to be any existing literature pertinent to the expansion-tube turbulent boundary-layer problem considered herein. For a plate located ahead of the secondary diaphragm, the problem is analogous to the shock-tube problem analyzed in references 5 and 6. For a plate located behind the secondary diaphragm, however, an accelerating-gas boundary layer is first established on the flat plate. This boundary layer is subsequently swept over by the interface separating the test gas and the acceler-

ating gas at two different temperatures. Finally, a test-gas boundary layer is established close to the leading edge of the plate. Whereas Mirels' problem (ref. 5) is steady in a shock-fixed coordinate system, the present problem is essentially time dependent. Thus, no semiempirical formulation (as used by Mirels and others) can be made.

MATHEMATICAL FORMULATION

Turbulent Compressible Boundary-Layer Equations

The basic differential equations describing the two-dimensional flow (with instantaneous values of velocity, density, and enthalpy) in a boundary layer on a flat plate (with the assumption of p_I = Constant) are (ref. 7):

Continuity:

$$\frac{\partial \rho_I}{\partial t} + \frac{\partial (\rho u)_I}{\partial x} + \frac{\partial (\rho v)_I}{\partial y} = 0 \tag{1}$$

Momentum:

$$\rho_I \left(\frac{\partial u_I}{\partial t} + u_I \frac{\partial u_I}{\partial x} + v_I \frac{\partial u_I}{\partial y} \right) = \frac{\partial}{\partial y} \left(\tau_{yx} \right)_I \tag{2}$$

Energy:

$$\rho_I \left(\frac{\partial h_I}{\partial t} + u_I \frac{\partial h_I}{\partial x} + v_I \frac{\partial h_I}{\partial y} \right) = \frac{\partial}{\partial y} \left(q_y \right)_I + \left(\tau_{yx} \right)_I \frac{\partial u_I}{\partial y} \tag{3}$$

where

$$\left(\tau_{yx} \right)_I = \left(\tau_{xy} \right)_I = \mu \frac{\partial u_I}{\partial y}$$

and

$$\left(q_y \right)_I = \frac{\mu}{N_{Pr}} \frac{\partial h_I}{\partial y} \tag{4}$$

Following Van Driest (ref. 7) the instantaneous values are separated into average and fluctuating components:

$$\left.\begin{aligned} u_I &= u + u' \\ \rho_I &= \rho + \rho' \\ h_I &= h + h' \\ T_I &= T + T' \\ v_I &= v + v' \\ \left(\tau_{yx}\right)_I &= \tau_{yx} + \tau'_{yx} \\ \left(q_y\right)_I &= q_y + q'_y \end{aligned}\right\} \tag{5}$$

The following averaging procedure is carried out with respect to time at a fixed point in space for a time-dependent mean flow. If Δt is a time interval much greater than the characteristic time scale associated with the fluctuations in a quantity $f(x,y,t)$, then the average value of $f(x,y,t)$ at a given point (see fig. 2(a)) is described by the equation

$$\bar{f}(x,y,t) = \frac{1}{\Delta t}\int_{t-\frac{\Delta t}{2}}^{t+\frac{\Delta t}{2}} f(x,y,t)dt \tag{6}$$

In case $\bar{f}(x,y,t)$ does not depend on the averaging interval Δt and physical time t, the mean value is said to be independent of time (see fig. 2(b)).

Introducing the expressions defined by equations (5) into equations (1) to (3), averaging with respect to time as defined by equation (6), and using the thin-boundary-layer assumptions, the following equations are obtained (see ref. 7 for details):

Continuity:

$$\frac{\partial \rho}{\partial t} + \frac{\partial(\rho u)}{\partial x} + \frac{\partial(\rho \tilde{v})}{\partial y} = 0 \tag{7}$$

Momentum:

$$\rho \frac{\partial u}{\partial t} + \rho u \frac{\partial u}{\partial x} + \rho \tilde{v} \frac{\partial u}{\partial y} = \frac{\partial}{\partial y}\left(\mu \bar{\epsilon} \frac{\partial u}{\partial y}\right) \tag{8}$$

Energy:

$$\rho \frac{\partial h}{\partial t} + \rho u \frac{\partial h}{\partial x} + \rho \tilde{v} \frac{\partial h}{\partial y} = \frac{\partial}{\partial y}\left(\frac{\mu}{N_{Pr}} \hat{\epsilon} \frac{\partial h}{\partial y}\right) + \mu \bar{\epsilon}\left(\frac{\partial u}{\partial y}\right)^2 \tag{9}$$

where

$$\tilde{v} = v + \frac{\overline{\rho' v'}}{\rho} \tag{10}$$

$$\bar{\epsilon} = 1 + \frac{\epsilon}{\mu} \tag{11}$$

$$\hat{\epsilon} = 1 + \frac{\epsilon}{\mu} \frac{N_{Pr}}{N_{Pr,t}} = 1 + \frac{k_T}{k} \tag{12}$$

The eddy viscosity has been defined as

$$\epsilon = -\rho \frac{\overline{u'v'}}{\partial u / \partial y} \tag{13}$$

and the eddy conductivity as

$$k_T = -\rho \frac{\overline{v'h'}}{\partial T / \partial y} \tag{14}$$

The static turbulent Prandtl number is defined as

$$N_{Pr,t} = c_p \frac{\epsilon}{k_T} \tag{15}$$

The following perfect-gas law is also introduced:

$$p = c_p\left(\frac{\gamma - 1}{\gamma}\right)\rho T \tag{16}$$

Other assumptions made are similar to those made in reference 2; namely,

(1) Since no general time-similar solution is possible, the problem is treated in two conically similar limits: (a) when the time-lag between arrival of the shock and the interface at the leading edge of the plate is very large (Blasius or BL limit), as shown in figure 3; (b) when this time lag is negligible (Mirels or MR limit); this limit is depicted in figure 4.

(2) The flow external to the boundary layer is not affected by the boundary-layer flow.

(3) The interface in the inviscid flow is considered to be thin.

(4) The wall temperature is assumed to be constant.

Transformed Plane

As pointed out in reference 2, the Crocco system of variables is suitable for treating time-unsteady problems such as the one to be treated here. In this system the independent variables are

$$\left.\begin{aligned} \bar{x} &\equiv x \\ \bar{u} &\equiv u(x,y,t) \\ \bar{t} &\equiv t \end{aligned}\right\} \tag{17}$$

and the dependent variables are

$$\left.\begin{aligned} \tau &= (\mu + \epsilon)\frac{\partial u}{\partial y} = \tau(\bar{x},\bar{u},\bar{t}) \\ h &= h(\bar{x},\bar{u},\bar{t}) \end{aligned}\right\} \tag{18}$$

In the conical coordinate system the independent variables (eqs. (17)) can be written as

$$\left.\begin{aligned} \alpha &= \frac{\bar{x}}{U_o t} \\ \beta &= \frac{\bar{u}}{U_o} \\ \bar{\gamma} &= \frac{\rho_w U_o^2 \bar{t}}{\mu_w} \end{aligned}\right\} \tag{19}$$

and the dimensionless dependent variables as

$$\bar{\phi}(\alpha,\beta,\bar{\gamma}) = \frac{\tau}{\rho_w U_o^2} \tag{20a}$$

$$H(\alpha,\beta,\bar{\gamma}) = \frac{h - h_w}{h_w} \tag{20b}$$

With the introduction of equations (17) to (20), equations (8) and (9) become, respectively,

$$\bar{\phi}^2 \frac{\partial^2 \bar{\phi}}{\partial \beta^2} + C\bar{\epsilon}\left(\frac{\alpha - \beta}{\bar{\gamma}} \frac{\partial \bar{\phi}}{\partial \alpha} - \frac{\partial \bar{\phi}}{\partial \bar{\gamma}}\right) = \bar{\phi}\left[\frac{\alpha - \beta}{\bar{\gamma}} \frac{\partial (C\bar{\epsilon})}{\partial \alpha} - \frac{\partial (C\bar{\epsilon})}{\partial \bar{\gamma}}\right] \tag{21}$$

$$\bar{\phi}^2\left[\frac{U_o^2}{h_w} + \frac{\partial}{\partial \beta}\left(\frac{\hat{\epsilon}}{\bar{\epsilon}} \frac{1}{N_{Pr}} \frac{\partial H}{\partial \beta}\right)\right] + \left(\frac{1}{N_{Pr}} \frac{\hat{\epsilon}}{\bar{\epsilon}} - 1\right)\bar{\phi} \frac{\partial \bar{\phi}}{\partial \beta} \frac{\partial H}{\partial \beta} = C\bar{\epsilon}\left(\frac{\partial H}{\partial \bar{\gamma}} - \frac{\alpha - \beta}{\bar{\gamma}} \frac{\partial H}{\partial \alpha}\right) \tag{22}$$

In obtaining equations (21) and (22), the continuity equation, equation (7), has been utilized.

To obtain self-similar solutions in the Crocco system, the following relations are assumed for $\bar{\phi}$, H, and C:

$$\bar{\phi}(\alpha,\beta,\bar{\gamma}) = \frac{\phi(\alpha,\beta)}{(\alpha\bar{\gamma})^{1/5}} \tag{23a}$$

$$\frac{\partial H}{\partial \gamma} = 0 \tag{23b}$$

thus $H = H(\alpha,\beta)$ and it follows that

$$\left.\begin{aligned} &\frac{\partial C}{\partial \bar{\gamma}} = 0 \\ &C = C(\alpha,\beta) \end{aligned}\right\} \tag{23c}$$

If the thermal-wall conditions are time dependent, then the assumptions contained in equations (23) cannot be made (see ref. 8 for details). In that case, the presence of three independent variables $(\alpha,\beta,\bar{\gamma})$ instead of two will substantially complicate the computation of the solutions. Presumably a step-by-step forward integration in the positive $\bar{\gamma}$ direction may be used to treat such problems.

Equations (21) and (22), with the use of equations (23), can now be written as

$$\phi^2 \frac{\partial^2 \phi}{\partial \beta^2} + \frac{C\bar{\epsilon}}{(\alpha\bar{\gamma})^{3/5}}\left[\alpha(\alpha - \beta)\frac{\partial \phi}{\partial \alpha} + \beta\frac{\phi}{5}\right] = \frac{\phi}{(\alpha\bar{\gamma})^{3/5}}\left[\alpha(\alpha - \beta)\frac{\partial (C\bar{\epsilon})}{\partial \alpha} - \alpha\bar{\gamma}\frac{\partial (C\bar{\epsilon})}{\partial \bar{\gamma}}\right] \tag{24}$$

$$\phi^2\left[\frac{U_o^2}{h_w} + \frac{\partial}{\partial \beta}\left(\frac{\hat{\epsilon}}{\bar{\epsilon}}\frac{1}{N_{Pr}}\frac{\partial H}{\partial \beta}\right)\right] + \left(\frac{1}{N_{Pr}}\frac{\hat{\epsilon}}{\bar{\epsilon}} - 1\right)\phi\frac{\partial \phi}{\partial \beta}\frac{\partial H}{\partial \beta} = \frac{C\bar{\epsilon}}{(\alpha\bar{\gamma})^{3/5}}\left[\alpha(\beta - \alpha)\frac{\partial H}{\partial \alpha}\right] \tag{25}$$

Further, in order to make equations (24) and (25) self-similar, it is necessary to assume the following relation for $\bar{\epsilon}$:

$$\bar{\epsilon}(\alpha\bar{\gamma},\alpha,\beta) = (\alpha\bar{\gamma})^{3/5}\,\bar{\bar{\epsilon}}(\alpha,\beta) \tag{26}$$

The validity of this equation will be discussed later.

The Incompressible data which are available for the core region of pipe flow and the outer regions of boundary layers (ref. 9) indicate that $N_{Pr,t}$ ranges between 0.7 and 0.9. For compressible flows, where very little data are available, Meier and Rotta (ref. 10)

found for $1.75 \leqq M_\infty \leqq 4.5$ that $N_{Pr,t}$ increased above unity for $y^* < 50$ (where $y^* = \frac{y\sqrt{\tau_w/\rho_w}}{\nu_w}$) and ranged between 0.8 and 0.85 as the outer edge of the boundary layer is approached.

In this analysis the molecular Prandtl number N_{Pr} and the turbulent Prandtl number $N_{Pr,t}$ will be assumed, for simplicity, to have the same constant value of 0.8. For this case

$$\bar{\epsilon} = \hat{\epsilon} \tag{27}$$

In view of the relations in equations (26) and (27), equations (24) and (25) finally yield

$$\phi^2 \frac{\partial^2 \phi}{\partial \beta^2} + \frac{4}{5} C\bar{\bar{\epsilon}}\beta\phi = \alpha(\beta - \alpha)\bar{\bar{\epsilon}}\left(C \frac{\partial \phi}{\partial \alpha} - \phi \frac{\partial C}{\partial \alpha}\right) - \alpha(\beta - \alpha)C\phi \frac{\partial \bar{\bar{\epsilon}}}{\partial \alpha} \tag{28}$$

$$\phi^2\left(\frac{U_o^2}{h_w} + \frac{1}{N_{Pr}} \frac{\partial^2 H}{\partial \beta^2}\right) + \left(\frac{1}{N_{Pr}} - 1\right)\phi \frac{\partial \phi}{\partial \beta} \frac{\partial H}{\partial \beta} = C\bar{\bar{\epsilon}}\left[\alpha(\beta - \alpha)\frac{\partial H}{\partial \alpha}\right] \tag{29}$$

BOUNDARY CONDITIONS

The various regions used in the specification of boundary conditions have been defined in reference 2. The same definitions will be used in this section. In the transformed plane the regions of interest in the BL (or Blasius) limit and the MR (or Mirels) limit have been shown in figures 5 and 6, respectively.

Shock Region (M) and Limited Interaction (LI) Region (Contained Between $\alpha^* = 1$ and $\alpha = 1$ in Figs. 3(b) and 5)

Boundary Conditions

First the shock region is considered. The separation-of-variables approach used for the laminar case (ref. 2) does not work for the turbulent case. In order to overcome this difficulty, the solutions for the shock region have been obtained in the shock-fixed coordinate system (fig. 7). The shock-region boundary layer in this coordinate system is time steady, and the solutions can easily be obtained. The following relations exist between the plate-fixed and shock-fixed systems:

$$x + x^+ = U_s t \tag{30}$$

$$U_o + U_e = U_s \tag{31}$$

$$\phi(\alpha,\beta) = \frac{\alpha^{1/5}(A - 1)^{4/5}}{(A - \alpha)^{1/5}} M^+(\beta) \tag{32}$$

$$H(\alpha,\beta) = H_M^+(\beta) \tag{33}$$

The equations governing $M^+(\beta)$ and $H_M^+(\beta)$ are (see appendix A for details):

$$M^+ \frac{d^2M^+}{d\beta^2} + \frac{4}{5}\tilde{\beta}\tilde{C}\tilde{\bar{\epsilon}}^+ = 0 \tag{34a}$$

$$M^+\left[\frac{1}{N_{Pr}}\frac{d^2H_M^+}{d\beta^2} + \frac{(U_e - U_s)^2}{h_w}\right] + \left(\frac{1}{N_{Pr}} - 1\right)\frac{dM^+}{d\beta}\frac{dH_M^+}{d\beta} = 0 \tag{34b}$$

The boundary conditions on $M^+(\beta)$ and $H_M^+(\beta)$ are

$$\left.\begin{aligned} \left.\frac{dM^+}{d\beta}\right|_{\beta=0} &= 0 \\ \left.M^+\right|_{\beta=1} &= 0 \end{aligned}\right\} \tag{35a}$$

$$\left.\begin{aligned} \left.H_M^+\right|_{\beta=0} &= 0 \\ \left.H_M^+\right|_{\beta=1} &= H_o = \frac{h_o - h_w}{h_w} \end{aligned}\right\} \tag{35b}$$

The solutions of equations (34a) and (34b) are used in relations (32) and (33) to provide the boundary conditions on ϕ and H at $\alpha = 1$ for the I region in the MR limit. The I-region boundary conditions on $\phi(\alpha^* = 1,\beta)$ and $H(\alpha^* = 1,\beta)$ for the BL limit are obtained by solving the steady-state forms of equations (28) and (29) (see eqs. (36a) (36b)) subject to the boundary conditions (37a) and (35b), respectively.

Leading-Edge Boundary Conditions

The boundary conditions at $\alpha^* = 0$ (BL limit) and at $\alpha = 0$ (MR limit) are provided by the solution of the steady turbulent boundary-layer equations for a flat plate. At $\alpha = 0$, $\phi = G(\beta)$ and, for an asymptotic approach to the steady state $\left.\frac{\partial \phi}{\partial \alpha}\right|_{\alpha=0} = 0$. The momentum equation (eq. 28) for such a case yields

$$G\frac{d^2G}{d\beta^2} + \frac{4}{5}C\bar{\bar{\epsilon}}\beta = 0 \tag{36a}$$

Similarly, by taking $H|_{\alpha=0} = H_G(\beta)$ and $\left.\frac{dH}{d\alpha}\right|_{\alpha=0} = 0$ the energy equation (eq. (29)) simplifies to

$$G\left(\frac{U_o^2}{h_w} + \frac{1}{N_{Pr}}\frac{d^2H_G}{d\beta^2}\right) + \left(\frac{1}{N_{Pr}} - 1\right)\frac{dG}{d\beta}\frac{dH_G}{d\beta} = 0 \tag{36b}$$

The boundary conditions on $G(\beta)$ and $H_G(\beta)$ are

$$\left.\begin{aligned} \left.\frac{dG}{d\beta}\right|_{\beta=0} &= 0 \\ G|_{\beta=1} &= 0 \end{aligned}\right\} \tag{37a}$$

$$\left.\begin{aligned} H_G|_{\beta=0} &= 0 \\ H_G|_{\beta=1} &= 0 \end{aligned}\right\} \tag{37b}$$

The BL-limit boundary conditions at $\alpha^* = 0$ can be obtained by replacing α by α^* in assumptions leading to equations (36) and (37).

Wall Boundary Conditions

For zero slip, impermeable wall, and constant wall temperature, the MR-limit boundary conditions on ϕ and H are

$$\left.\begin{aligned} \frac{d\phi}{d\beta}(\alpha,\beta = 0) &= 0 \\ H(\alpha,\beta = 0) &= 0 \end{aligned}\right\} \qquad \left(0 \leqq \alpha \leqq 1\right) \tag{38}$$

The wall boundary conditions for the BL limit may be obtained from equations (38) by replacing α by α^*.

Boundary-Layer Edge or Free-Stream Condition

For MR limit the free-stream boundary conditions on ϕ and H are

$$\left.\begin{aligned} \phi(\alpha,\beta = 1) &= 0 \\ H(\alpha,\beta = 1) &= 0 \end{aligned}\right\} \qquad \left(0 \leqq \alpha \leqq 1\right) \tag{39}$$

Once again, the BL-limit boundary conditions may be obtained by using α^* in place of α in the equations (39).

In equations (39) the free-stream temperature (between the interface and the expansion fan) has been taken equal to the plate temperature. This assumption is appropriate for expansion-tube flow duplication studies (ref. 11). For simulation studies equations (39) should be modified for relevant values of H in free stream.

The values of the parameters A, U_o^2/h_w, and T_o/T_w required in obtaining the boundary conditions and for solving the governing equations have been obtained from the inviscid shock-tube relations (see appendix B).

TURBULENT TRANSPORT MODEL

Following references 4 and 9, the turbulent boundary layer is treated as a composite layer characterized by inner and outer regions. In the inner region, an eddy viscosity based on Prandtl's mixing-length theory is used; in the outer region, a nearly constant eddy viscosity based on the Clauser model (ref. 9) is used. It is exactly constant when the flow is incompressible and without heat transfer. The intermittent character of the outer region is accounted for by using an intermittency factor.

Viscosity in the Inner Region

The eddy viscosity for the inner region referenced to the molecular viscosity is obtained from (ref. 4)

$$\left(\frac{\epsilon}{\mu}\right)_i = \frac{\rho K_1^2 y^2}{\mu}\left[1 - \exp\left(-\sqrt{\frac{\nu_w}{\bar{\nu}}}\frac{y}{A}\right)\right]^2 \left|\frac{\partial u}{\partial y}\right| \tag{40}$$

where $A = 26\nu_w\left(\frac{\rho_w}{\tau_w}\right)^{1/2}$ and $\bar{\nu}$ is the mean value of ν taken over the viscous sublayer. As an approximation the ratio of $\nu_w/\bar{\nu}$ is assumed to be unity.

Viscosity in the Outer Region

The ratio of the eddy viscosity to the molecular viscosity in the outer region can be expressed as (ref. 4)

$$\left(\frac{\epsilon}{\mu}\right)_o = K_2 \frac{\rho U_o}{\mu} \delta^*_{inc} \bar{\bar{\gamma}} \tag{41}$$

where δ^*_{inc} is the incompressible displacement thickness

$$\delta^*_{inc} = \int_0^{y_e} \left(1 - \frac{u}{U}\right)_o dy \tag{42}$$

and the intermittency factor $\bar{\bar{\gamma}}$ is given by

$$\bar{\bar{\gamma}} = \frac{1 - \operatorname{erf} 5\left(\frac{y}{\delta} - 0.78\right)}{2} \tag{43}$$

In this expression δ is the thickness of the boundary layer.

Matching Procedure

The criterion of the continuity of eddy viscosity gives the following relations for the matching at the boundary between the inner and outer regions:

$$\left.\begin{aligned}\left(\frac{\epsilon}{\mu}\right)_i &= \frac{\rho K_1^2 y^2}{\mu}\left\{1 - \exp\left[-\left(\frac{\nu_w}{\nu}\right)^{1/2}\frac{y}{A}\right]\right\}^2\left|\frac{\partial u}{\partial y}\right| && (0 \leq y \leq y_m)\\ \left(\frac{\epsilon}{\mu}\right)_o &= \frac{\rho K_2 U_o}{\mu}\delta^*_{inc}\,\bar{\bar{\gamma}} && (y > y_m)\end{aligned}\right\} \tag{44}$$

where y_m is determined from

$$\left(\frac{\epsilon}{\mu}\right)_i = \left(\frac{\epsilon}{\mu}\right)_o \tag{45}$$

Transformed Models

From equations (18), (20), and (23) the following expression may be obtained

$$\frac{\partial u}{\partial y} = \frac{\rho_w U_o^2}{\mu + \epsilon}\frac{\phi}{(\alpha\bar{\gamma})^{1/5}} \tag{46}$$

which, upon integration, gives

$$y = \frac{(R_{w,x})^{1/5}}{\rho_w U_o}\int_0^\beta \frac{C\mu_w(H+1)\bar{\epsilon}}{\phi}\,d\xi \tag{47}$$

Equation (47) may finally be written as

$$y = (R_{w,x})^{1/5}\left(\frac{\mu_w}{U_o}\right)\left(\frac{h_w}{p_o}\right)\left(\frac{\gamma - 1}{\gamma}\right)\int_0^\beta\left[\frac{C\bar{\epsilon}}{\phi}(H+1)\right]d\xi \tag{48}$$

Substitution of expressions (46) and (48) in equation (40) results in

$$\left(\frac{\epsilon}{\mu}\right)_i\left(1 + \frac{\epsilon}{\mu}\right)_i = \frac{K_1^2 I^2}{C^2(H+1)^3}(R_{w,x})^{1/5}\left\{1 - \exp\left[-(R_{w,x})^{1/10}\sqrt{\phi_w}\,\frac{I}{26}\right]\right\}^2|\phi| \tag{49}$$

where the following relations have also been used (from perfect-gas relations and boundary-layer approximations):

$$\left.\begin{aligned}
&\frac{\tau}{\rho_w U_o^2} = \frac{\phi}{\left(R_{w,x}\right)^{1/5}} \\
&\frac{\rho_w h_w}{p_o}\frac{\gamma - 1}{\gamma} = 1 \\
&C = \frac{\mu\rho}{\mu_w \rho_w} \\
&\frac{\rho}{\rho_w} = \frac{1}{H + 1} \\
&I = \int_0^{\beta} \frac{C\bar{\epsilon}}{\phi}(H + 1)d\xi
\end{aligned}\right\} \tag{50}$$

Equation (49) is quadratic in $(\epsilon/\mu)_i$ and, therefore, has two solutions for $(\epsilon/\mu)_i$. It is easy to see, however, that $(\epsilon/\mu)_i$ goes to zero as y goes to zero only if the positive root is taken. Hence, the relation for $(\epsilon/\mu)_i$ is obtained as

$$\left(\frac{\epsilon}{\mu}\right)_i = \frac{-1 + \left\{1 + 4\left[\frac{K_1^2 I^2}{C^2(H + 1)^3}\left(R_{w,x}\right)^{1/5}\left\{1 - \exp\left[-\left(R_{w,x}\right)^{1/10}\sqrt{\phi_w}\,\frac{I}{26}\right]\right\}^2 |\phi|\right]\right\}^{1/2}}{2} \tag{51}$$

Similarly the eddy-viscosity equation (eq. (41)) for the outer region can be written in the transformed plane as

$$\left(\frac{\epsilon}{\mu}\right)_o = \frac{1}{C}\frac{1}{(H + 1)^2}\frac{K_2 J}{2}\left(R_{w,x}\right)^{1/5}\left[1 - \operatorname{erf} 5\left(\frac{I}{I_{0.99}} - 0.78\right)\right] \tag{52}$$

where

$$\left.\begin{aligned} I &= \int_0^{\beta} \frac{C\bar{\epsilon}}{\phi}(H + 1)d\xi \\ J &= \int_0^{0.99} (1 - \beta)\frac{C\bar{\epsilon}}{\phi}(H + 1)d\beta \end{aligned}\right\} \tag{53}$$

Now, when the exponential term of equation (40) is expanded and a logarithmic approximation is used for the velocity profile, it is found that $(\epsilon/\mu)_i$ varies as y^3. Of course, such a logarithmic approximation is assumed to be valid only for small values of y lying in the region between the laminar sublayer and the region where the classical logarithmic law with a different slope is often applied. Hence, from equation (47) it may be said that $(\epsilon/\mu)_i$ varies as $\left(R_{w,x}\right)^{3/5}$.

In order to make equations (24) and (25) self-similar, relation (26) was employed. The relation in equation (26) gives the following Reynolds number dependence for $(\epsilon/\mu)_i$:

$$\bar{\epsilon}_i\left(R_{w,x},\alpha,\beta\right) = \left(R_{w,x}\right)^{3/5}\bar{\bar{\epsilon}}_i(\alpha,\beta) \tag{54a}$$

and the further approximation is introduced

$$\bar{\bar{\epsilon}}_i(\alpha,\beta) \approx \frac{1}{\left(R_{w,L}\right)^{3/5}} + \frac{(\epsilon/\mu)_i}{\left(R_{w,x}\right)^{3/5}} \tag{54b}$$

where $(\epsilon/\mu)_i$ is evaluated from equation (51) and $R_{w,L}$ is evaluated at $x = L$, which is the average length of the model. This approximation is not valid for $x \ll L$ but is used since the basic assumption of turbulent flow is on no firmer grounds.

In order to make equation (52) compatible with relation (26), equation (52) is approximated as

$$\left(\frac{\epsilon}{\mu}\right)_o \approx \frac{1}{C}\frac{1}{(H + 1)^2}\frac{K_2}{\left(R_{w,L}\right)^{2/5}}\left(R_{w,x}\right)^{3/5}\frac{J}{2}\left[1 - \text{erf } 5\left(\frac{I}{I_{0.99}} - 0.78\right)\right] \tag{55}$$

so that

$$\bar{\bar{\epsilon}}_o(\alpha,\beta) \approx \frac{(\epsilon/\mu)_o}{\left(R_{w,x}\right)^{3/5}} \approx \frac{1}{C}\frac{1}{(H + 1)^2}\frac{K_2}{\left(R_{w,L}\right)^{2/5}}\frac{J}{2}\left[1 - \text{erf } 5\left(\frac{I}{I_{0.99}} - 0.78\right)\right] \tag{56}$$

Before closing this section it should be pointed out that the assumptions made in obtaining expressions (54) and (56) are further additions to the original assumptions contained in expressions (40) and (41), which themselves are also approximate. For lack of anything better, however, these relations are employed and their validity checked against some time-steady experimental data. The validity of these results for the unsteady flow still needs experimental substantiation of equations (54) and (56).

SOLUTION OF THE GOVERNING EQUATIONS

Numerical Procedure

The numerical solution of the boundary-value problem (eqs. (28) and (29)) formulated in this work is sought by using the Gauss-Seidel line-relaxation method. The finite-differencing scheme and the method of linearization used here closely parallel that of reference 2.

By using the central difference approximations (see ref. 2) equations (28) and (29) may be written as follows for solutions along lines of constant β (the superscript p refers to the iteration number):

$$\left[\frac{h\alpha_m(\alpha_m - \beta_n)\bar{\epsilon}_{m,n}C_{m,n}}{4\left(\phi^{p-1}_{m,n}\right)^2 - \frac{8}{5}C_{m,n}\bar{\epsilon}_{m,n}\beta_n}\right]\phi^p_{m-1,n} + \phi^p_{m,n} - \left[\frac{h\alpha_m(\alpha_m - \beta_n)\bar{\epsilon}_{m,n}C_{m,n}}{4\left(\phi^{p-1}_{m,n}\right)^2 - \frac{8}{5}C_{m,n}\bar{\epsilon}_{m,n}\beta_n}\right]\phi^p_{m+1,n} = -\frac{h\alpha_m(\alpha_m - \beta_n)\phi^{p-1}_{m,n}}{4\left(\phi^{p-1}_{m,n}\right)^2 - \frac{8}{5}h^2C_{m,n}\bar{\epsilon}_{m,n}\beta_n}\left[\bar{\epsilon}_{m,n}\left(C_{m+1,n} - C_{m-1,n}\right) + C_{m,n}\left(\bar{\epsilon}_{m+1,n} - \bar{\epsilon}_{m-1,n}\right)\right] + \frac{\left(\phi^{p-1}_{m,n}\right)^2}{2\left(\phi^{p-1}_{m,n}\right)^2 - \frac{4}{5}h^2C_{m,n}\bar{\epsilon}_{m,n}\beta_n}\left(\phi^{p-1}_{m,n+1} + \phi^p_{m,n-1}\right) \tag{57}$$

$$\left[\frac{hN_{Pr}}{4\phi^2_{m,n}}\bar{\epsilon}_{m,n}C_{m,n}\alpha_m(\alpha_m - \beta_n)\right]H^p_{m-1,n} + H^p_{m,n} - \left[\frac{hN_{Pr}}{4\phi^2_{m,n}}\bar{\epsilon}_{m,n}C_{m,n}\alpha_m(\alpha_m - \beta_n)\right]H^p_{m+1,n} = \frac{h^2N_{Pr}}{2}\frac{U_o^2}{h_w} + \frac{1}{2}\left(H^{p-1}_{m,n+1} + H^p_{m,n-1}\right) + \frac{N_{Pr}}{8\phi_{m,n}}\left(\frac{1}{N_{Pr}} - 1\right)\left(\phi_{m,n+1} - \phi_{m,n-1}\right)\left(H^{p-1}_{m,n+1} - H^p_{m,n-1}\right) \tag{58}$$

In equations (57) and (58) the nonlinearities have been removed by using values of the dependent variables from the previous iteration in the coefficients. Each of equations (57) and (58) forms a set of $\left(\frac{1}{h} - 1\right)$ simultaneous difference equations for a given value of n when m varies from 2 to $1/h$. Since the coefficient matrix of each of these equations is of the tridiagonal form, the Thomas algorithm of reference 12 may be employed.

The numerical solution is started by calculating the fluid properties and establishing the inner and outer regions from laminar ϕ and H distributions. The momentum equation (eq. (57)) is now solved iteratively for a new ϕ distribution along lines of constant β for the whole flow field until

$$\left| \frac{\phi_w^p - \phi_w^{p-1}}{\phi_w^{p-1}} \right| < \epsilon_1^*$$

where ϵ_1^* is of the order of 10^{-5}. This value of p is taken as p_{max}.

Next, equation (58) is solved iteratively in the same manner p_{max} times. The improved $\phi^{p_{max}}$ and $H^{p_{max}}$ distributions are now used to calculate the new fluid properties and establish inner and outer regions. With these values the momentum and the energy equations are solved again. This process is continued until convergence to the desired accuracy

$$\left| \frac{\phi^J(\alpha,0) - \phi^{J-1}(\alpha,0)}{\phi^{J-1}(\alpha,0)} \right| < \epsilon_o^*$$

is obtained. Here ϵ_o^* is a small number of the order of 10^{-5} and J is the iteration number.

The convergence rate of the solutions can be improved substantially if equations (57) and (58) are solved first for a coarse mesh ($h = 0.1$), and then with linear interpolation these coarse solutions are used as initial guesses in the iteration with fine mesh ($h = 0.01$). A computer flow chart for the procedure used is given in figure 8.

Calculated Boundary-Layer Parameters

Once the ϕ and H distributions from the numerical solutions are obtained, the boundary-layer parameters, such as local skin-friction coefficient, Stanton numbers, and boundary-layer thickness, can easily be obtained. Some of these parameters are given by the following equations. The local skin-friction coefficient is given by

$$c_f = \frac{\tau_w}{\frac{1}{2}\rho_w U_o^2} \tag{59}$$

where

$$\tau_w = \mu_w \left(\frac{\partial u}{\partial y}\right)_{y=0}$$

From equations (20) and (23)

$$\frac{\tau_w}{\rho_w U_o^2} = \frac{\phi_w}{(\alpha\bar{\gamma})^{1/5}} \tag{60}$$

Hence,

$$c_f = \frac{2\phi_w}{(\alpha\bar{\gamma})^{1/5}}$$

or,

$$c_f \left(R_{w,x}\right)^{1/5} = 2\phi_w \tag{61}$$

The heat transfer at the wall can be obtained from

$$q_w = -k_w \left(\frac{\partial T}{\partial y}\right)_w \tag{62}$$

In terms of the transformed variables, this result can be further written as

$$q_w = \frac{\rho_w U_o h_w}{N_{Pr}} \frac{\phi}{(\alpha\bar{\gamma})^{1/5}} \left(\frac{\partial H}{\partial \beta}\right)_w \tag{63}$$

Defining the Stanton number as

$$N_{St} = -\frac{q_w}{\rho_w U_o c_p \left(T_r - T_w\right)} \tag{64}$$

equation (63) becomes

$$N_{St} = \frac{1}{N_{Pr}} \frac{\phi_w}{(\alpha\bar{\gamma})^{1/5}} \left(\frac{\partial H}{\partial \beta}\right)_w \frac{1}{\frac{T_r}{T_w} - 1} \tag{65}$$

where the recovery temperature T_r is obtained from the ratios

$$\left.\begin{aligned} r &= \frac{T_r - T_\infty}{T_{st} - T_\infty} \\ r &= \left(N_{Pr}\right)^{1/3} \end{aligned}\right\} \tag{66}$$

The assumption of $r = \left(N_{Pr}\right)^{1/3}$ has no firm basis for such unsteady flows and is probably inaccurate. It is used here simply to permit expression of the results in terms of a Stanton number. With

$$T_{st} = T_\infty + \frac{U_o^2}{2c_p}$$

and

$$T_\infty = T_w$$

expressions (66) yield

$$\frac{T_r}{T_w} - 1 = \left(N_{Pr}\right)^{1/3} \frac{U_o^{\,2}}{2h_w} \tag{67}$$

From equations (65) and (67) the following expression is obtained for the Stanton number

$$N_{St}\left(R_{w,x}\right)^{1/5} = \frac{2h_w}{U_o^{\,2}} \frac{\phi_w}{\left(N_{Pr}\right)^{4/3}\left(\frac{\partial H}{\partial \beta}\right)_w} \tag{68}$$

Inversion to Physical Plane

From the definition of the transformed variables

$$\tau = \rho_w U_o^{\,2} \frac{\phi}{(\alpha\bar{\gamma})^{1/5}}$$

or

$$\frac{\partial u}{\partial y} = \left(\frac{\rho_w^{\,4} U_o^{\,9} \mu_w}{x}\right)^{1/5} \frac{\phi}{\mu + \epsilon} \tag{69}$$

so that

$$y(\alpha,\beta) = \frac{x^{1/5}}{\left(\rho_w^{\,4} U_o^{\,4} \mu_w\right)^{1/5}} \int_0^{\beta} \frac{\mu}{\phi} \bar{\epsilon}\, d\xi \tag{70}$$

Now

$$\mu = C\mu_w \rho_w \frac{R}{p_o} \frac{h_w}{c_p}(H + 1) \tag{71}$$

Hence, from equation (70) the dimensionless ordinate η may be written as

$$\eta(\alpha,\beta) = \frac{y}{\left(\frac{x^4 \tilde{\rho}_w {}^4 \mu_w}{U_o}\right)^{1/5} \frac{\gamma - 1}{\gamma} \frac{h_w}{p_o}} = \int_0^\beta \frac{C(H + 1)\bar{\bar{\epsilon}}}{\phi} \, d\xi \tag{72}$$

where $\bar{\bar{\epsilon}}$ is related to $\bar{\epsilon}$ by the expression in equation (26).

By evaluating the integral appearing in equation (72) at fixed α for various β values, the profiles of $\eta\left(\alpha, \frac{u}{U_o}\right)$ at various α values can be obtained. These may be used to obtain velocity profiles $\frac{u}{U_o}(\eta)$ for various values of α.

The temperature in the boundary layer may be obtained from

$$T = \frac{h_w}{c_p}(H + 1) \tag{73}$$

From equation (72)

$$\frac{y}{\delta} = \frac{\eta}{\eta_{0.99}} = \frac{\int_0^\beta \frac{C(H + 1)\bar{\bar{\epsilon}}}{\phi} \, d\xi}{\int_0^{0.99} \frac{C(H + 1)\bar{\bar{\epsilon}}}{\phi} \, d\xi} \tag{74}$$

may also be obtained.

DISCUSSION OF RESULTS

Evaluation of Some Numerical Results and Comparison With Experimental Data

Some of the numerical results for skin-friction drag for a fully turbulent boundary layer on a flat plate are compared herein with the experimental data of Moore and Harkness (ref. 13). The experimental results were obtained on a sharp-leading-edge flat-plate model with a floating-element-type balance for $1 \times 10^7 < R_{\infty,x} < 2 \times 10^8$. The test conditions were as follows:

$M_\infty = 2.8$

$p_{t,\infty} = 0.9997 \times 10^6$ N/m^2

$T_{t,\infty} = 311.1$ K

$$\frac{T_w}{T_{t,\infty}} = 0.947$$

The governing equations, equations (28) and (29), reduce to the time-steady flat-plate fully turbulent boundary-layer equations for $\alpha = 0$. The numerical results of these equations, solved to obtain the local skin-friction coefficient, are compared with the experimental data in figure 9.

The agreement is good at high Reynolds numbers and fair at lower Reynolds numbers. Note that the value of the reference Reynolds number, $R_{w,L}$, used in the computations is 1×10^7. For the range of $R_{e,x}$ considered in figure 9, x/L varies from 0.4 to 4.

Time-Dependent Results

The skin-friction, heat-transfer, velocity, and temperature profiles have been obtained for a wave-induced compressible turbulent boundary layer on a flat plate after passage of an interface with application to expansion-tube flows. The gas considered on the two sides of the interface is "perfect" nitrogen. The results presented correspond to a free-stream velocity of 6 km/sec with a shock Mach number of 20.8. A reference Reynolds number of 3.78×10^6 per meter is employed in expressions (54) and (56). This value corresponds to the following conditions:

$p_w = 10^3$ N/m^2

$U_o = 6$ km/sec

$T_w = 300$ K

$\mu_w = 1.785 \times 10^{-5}$ N-sec/m^2

The molecular and the turbulent Prandtl numbers are assumed to have the same constant value of 0.8. The plate as well as the free stream behind the interface is

assumed to be at the same temperature, 300 K, for this analysis; this assumption is pertinent to flow-duplication studies (ref. 11).

Figures 10 and 11 give the local skin-friction coefficient for the MR and BL limits, respectively. In both of these figures the skin-friction coefficient relaxes to within 6 percent of the steady-state value at $\alpha = 0.6$. Shown in the following table are the wall skin-friction coefficients computed by the Spalding-Chi correlation (ref. 14), by the Van Driest method (ref. 7), and by the Schultz-Grunow method (ref. 15) employing the Eckert reference temperature approach to account for compressibility. It may be noted here that the present problem produces $c_f\left(R_{W,x}\right)^{1/5} = \text{Constant}$ for the steady state, whereas the other methods do not.

For $\alpha = 0$ (steady-state results)				
$R_{e,x}$	Spalding-Chi (ref. 14)	Schultz-Grunow (ref. 15)	Van Driest (ref. 7)	Present
$c_f\left(R_{e,x}\right)^{1/5}$ for $\frac{T_w}{T_e} = 1$; $M_e \approx 17$; $T_w = 300$ K				
1.17×10^6	6.054×10^{-3}	11.26×10^{-3}	10.55×10^{-3}	9.22×10^{-3}
1.17×10^7	6.880	10.40	10.80	
1.78×10^8	8.420	10.67	12.00	
$N_{St}\left(R_{e,x}\right)^{1/5}$ for $\frac{T_w}{T_e} = 1$; $M_e \approx 17$; $T_w = 300$ K				
1.17×10^6	3.27×10^{-3}	6.43×10^{-3}	5.86×10^{-3}	4.8×10^{-3}
1.17×10^7	3.67	5.75	5.86	
1.78×10^8	4.44	5.76	6.43	

The Stanton number distribution for the MR and BL limits is also shown in figures 10 and 11, respectively. These figures indicate that the wall heat transfer relaxes to (within 6 percent) its final steady-state value at $\alpha = 0.5$. The high $\left(\frac{\partial H}{\partial \beta}\right)_w$ values in the vicinity of $\alpha = 1$ result from the imposed temperature boundary condition. Also shown in the preceding table are the Stanton number values computed by using the previously quoted skin-friction relations from references 7, 14, and 15 and the Reynolds analogy.

Since this work was started with the aim of determining how a wave-induced boundary layer would relax if it were assumed turbulent instead of laminar from the beginning

of its formation, a brief comparison with the laminar results is of interest. It was shown in references 2 and 3 that for a laminar boundary layer the Stanton number and the local skin-friction coefficient relax to within about 6 percent of the steady-state value of $\alpha = 0.3$ (for the same free-stream velocity and temperature values). The present work indicates that a fully turbulent boundary layer relaxes faster to the time-steady values as compared to a laminar boundary layer. This result should be expected from the enhanced transfer of momentum and energy in a turbulent boundary layer. The result is also supported by the work of Trimpi and Cohen (ref. 6). They showed that the slope of the boundary-layer characteristic which bounds the steady-state is controlled by the ratio $\delta^*_{inc}/\theta_{inc}$. The Blasius value of this ratio for the laminar case (n = 1) is 2.6 and for the turbulent case (n = 7) is 1.29. These values imply that the slope of the boundary-layer characteristics is smaller when compared to the laminar boundary layer. Hence the turbulent boundary layer should relax faster as indicated by limiting values of $\alpha \approx 0.39$ and 0.77 (reciprocals of 2.6 and 1.29) for the laminar and fully turbulent cases, respectively.

Figures 12 and 13 show the velocity and temperature distributions through the boundary layer for the MR limit. Note that at $\alpha = 0.6$ although the velocity profile has nearly reached its asymptotic shape throughout the entire boundary layer, the outer part of the temperature profile is still in the process of significant relaxation.

The wave-induced boundary-layer behavior can be interpreted in two different ways under the conical assumption. The present results are presented for the development of the boundary layer with time at a given x position on the plate ("fixed x"). A description of the boundary layer at any point in time ("fixed time") is often desirable. The Crocco conical coordinates (employed here) readily permit interpretation of results for either point of view. For the fixed-time point of view care should be taken in obtaining the results at the leading edge and at the shock wave since the boundary-layer equations are singular at both of these locations. When the fixed x point of view is taken, the product $\alpha\bar{\gamma}$ produces a Reynolds number which permits interpretation for fixed values of x, and in such a case α becomes a time variable. For the fixed-time point of view, $\bar{\gamma}$ is fixed and α becomes a position variable.

CONCLUDING REMARKS

Crocco variables have been employed to obtain time-similar (or conical) solutions of the wave-induced flow over a flat plate in an expansion tube. The boundary-layer flow was assumed to be fully turbulent. Results presented correspond to two limiting cases in which the flow external to the boundary layer can be considered similar in time or "conical." All intermediate cases should lie within the range of these two limits.

From these results, it is seen that the fully turbulent boundary layer relaxes faster to the time-steady state when compared to the laminar boundary layer. For the cases analyzed herein the turbulent boundary layer relaxes to the final steady-state values (within about 6 percent) of skin-friction and Stanton number over a length, measured from the leading edge of the plate, equal to about one-half of the distance traversed by the interface (separating cold and hot sections of the flow field) in the free stream.

The assumptions and approach were checked against steady-flow data and found to give a fairly good estimate of the local skin friction and heat transfer.

Langley Research Center,
National Aeronautics and Space Administration,
Hampton, Va., April 16, 1974.

APPENDIX A

SOLUTION OF THE SHOCK-REGION GOVERNING EQUATIONS

Since the separation-of-variables technique, used in the laminar case (ref. 2), was apparently not successful in the plate-fixed coordinate system, the solution for the shock-region (M) governing equations has been sought in the shock-fixed coordinate system. These results were later transferred to the plate-fixed system. (A similar treatment for the laminar case is given in ref. 16.)

As depicted in figure 7(a), the shock wave is moving with a velocity U_S and the fluid behind it with a velocity U_O. If the shock wave is fixed by subtracting U_S from every part of the flow field (including the wall), the flow shown in figure 7(b) results. This transformation to a shock-fixed coordinate system removes the unsteady character of the problem (for the portion of the flow field which is not influenced by the leading edge) present in the plate-fixed reference frame. The problem can now be treated by analyzing the steady-state turbulent boundary-layer equations for a flat plate.

Continuity:

$$\frac{\partial(\rho^+ u^+)}{\partial x^+} + \frac{\partial(\rho^+ \tilde{v}^+)}{\partial y^+} = 0 \tag{A1}$$

with

$$\tilde{v}^+ = v^+ + \frac{\overline{\rho' v'}^+}{\rho^+}$$

Momentum:

$$(\rho^+ u^+)\frac{\partial u^+}{\partial x^+} + \left(\rho^+ \tilde{v}^+\right)\frac{\partial u^+}{\partial y^+} = \frac{\partial}{\partial y^+}\left(\mu^+ \bar{\epsilon}^+ + \frac{\partial u^+}{\partial y^+}\right) \tag{A2}$$

with

$$\bar{\epsilon}^+ = 1 + \frac{\epsilon^+}{\mu^+}$$

APPENDIX A

Energy:

$$(\rho^+ u^+)\frac{\partial h^+}{\partial x^+} + (\rho^+ \tilde{v}^+)\frac{\partial h^+}{\partial y^+} = \frac{\partial}{\partial y^+}\left(\frac{\mu^+}{N_{Pr}}\hat{\epsilon}^+ + \frac{\partial h^+}{\partial y^+}\right) + \mu^+ \bar{\epsilon}^+ \left(\frac{\partial u^+}{\partial y^+}\right)^2 \tag{A3}$$

with

$$\hat{\epsilon}^+ = 1 + \frac{\epsilon^+}{\mu^+}\frac{N_{Pr}}{N_{Pr,t}}$$

The following definitions of the dependent and the independent variables are now employed in the Crocco system:

Dependent variables:

$$\left.\begin{aligned} \tau^+ &= \left(\mu^+ + \epsilon^+\right)\frac{\partial u^+}{\partial y^+} \\ h^+ &= h^+\left(\bar{x}^+, \bar{u}^+\right) \end{aligned}\right\} \tag{A4}$$

Independent variables:

$$\left.\begin{aligned} \bar{x}^+ &\equiv x^+ \\ \bar{u}^+ &\equiv u^+(x^+, y^+) \end{aligned}\right\} \tag{A5}$$

In terms of the Crocco variables, equations (A2) and (A3) may be written as

$$\frac{\partial^2 \tau^+}{\partial \bar{u}^{+2}} + \bar{u}^+ \frac{\partial}{\partial x^+}\left(\rho^+ \frac{\mu^+ \bar{\epsilon}^+}{\tau^+}\right) = 0 \tag{A6}$$

$$(\rho^+ \bar{u}^+)\mu^+ \bar{\epsilon}^+ \frac{\partial h^+}{\partial \bar{x}^+} = \tau^{+2}\left[1 + \frac{\partial}{\partial \bar{u}^+}\left(\frac{\hat{\epsilon}^+}{\bar{\epsilon}^+}\frac{1}{N_{Pr}}\frac{\partial h^+}{\partial \bar{u}^+}\right)\right] + \frac{1}{2}\left(\frac{1}{N_{Pr}}\frac{\hat{\epsilon}^+}{\bar{\epsilon}^+} - 1\right)\frac{\partial \tau^{+2}}{\partial \bar{u}^+}\frac{\partial h^+}{\partial \bar{u}^+} \tag{A7}$$

APPENDIX A

The following dimensionless variables are now introduced:

$$\left.\begin{aligned} \bar{\phi}^+ &= \frac{\tau^+}{\rho_w^+ U_e^{\,2}} \\ \beta &= \frac{U_w - \bar{u}^+}{U_w - U_e} \\ H &= \frac{h^+ - h_w^+}{h_w^+} \end{aligned}\right\} \tag{A8}$$

The momentum equation (eq. (A6)) and the energy equation (eq. (A7)) then become, respectively,

$$\frac{1}{\left(1 - \frac{U_w}{U_e}\right)^2} \frac{\partial^2 \bar{\phi}^+}{\partial \beta^2} + \tilde{\beta} C \frac{\mu_w^+}{\rho_w^+ U_e} \frac{\partial}{\partial \bar{x}^+}\left(\frac{\bar{\epsilon}^+}{\bar{\phi}^+}\right) = 0 \tag{A9}$$

$$\frac{\mu^+ \rho^+ \bar{\epsilon}^+}{\rho_w^{+2} U_e^{\,3}} \tilde{\beta}\left(U_e - U_w\right)^2 \frac{\partial H}{\partial \bar{x}^+} = \bar{\phi}^+ 2\left[\frac{\left(U_e - U_w\right)^2}{h_w} + \frac{\partial}{\partial \beta}\left(\frac{\hat{\epsilon}^+}{\bar{\epsilon}^+} \frac{1}{N_{Pr}} \frac{\partial H}{\partial \beta}\right)\right] + \left(\frac{1}{N_{Pr}} \frac{\hat{\epsilon}^+}{\bar{\epsilon}^+} - 1\right) + \frac{\partial \bar{\phi}^+}{\partial \beta} \frac{\partial H}{\partial \beta} \tag{A10}$$

where

$$\tilde{\beta} = \frac{U_w}{U_e} + \frac{U_e - U_w}{U_e} \beta$$

The following forms for $\bar{\phi}^+$ and $\bar{\epsilon}^+$ are now introduced so that the momentum equation (eq. (A9)) becomes independent of $\bar{x}^+$:

$$\bar{\phi}^+ = \left(1 - \frac{U_w}{U_e}\right)\left(\frac{\mu_w^+}{\rho_w^+ U_e \bar{x}^+}\right)^{1/5} M^+(\beta) \tag{A11}$$

$$\bar{\epsilon}^{+} = \left(\frac{\rho_w^{+} U_e \bar{x}^{+}}{\mu_w^{+}} \right)^{3/5} \bar{\bar{\epsilon}}^{+}(\beta) \tag{A12}$$

For the energy equation (eq. (A10)) it is assumed that

$$H = H(\beta) \tag{A13}$$

By using expressions (A11) to (A13) in equations (A9) and (A10) the following form of the shock-region governing equations is obtained:

$$M^{+} \frac{d^2 M^{+}}{d\beta^2} + \frac{4}{5} \tilde{\beta} C \bar{\bar{\epsilon}}^{+} = 0 \tag{A14}$$

$$M^{+} \left[\frac{(U_e - U_w)^2}{h_w^{+}} + \frac{1}{N_{Pr}} \frac{d^2 H}{d\beta^2} \right] + \left(\frac{1}{N_{Pr}} - 1 \right) \frac{dM^{+}}{d\beta} \frac{dH}{d\beta} = 0 \tag{A15}$$

In obtaining equation (A15) it is assumed that $N_{Pr} \approx N_{Pr,t} = 0.8$. The preceding assumption implies $\hat{\epsilon}^{+} = \bar{\epsilon}^{+}$.

It should be noted here that the nondimensional local enthalpy H has the same value in the plate and shock-fixed reference frames; however, the shear function $M^{+}(\beta)$ is to be related to the shear function $\phi(x,\beta)$ in the plate-fixed reference system.

Now, $\bar{\phi}$ by definition is

$$\bar{\phi} = \frac{\tau}{\rho_w U_o^{\,2}} = \left(\frac{\tau}{\rho_w U_e^{\,2}} \right) \left(\frac{U_e^{\,2}}{U_o^{\,2}} \right) \tag{A16}$$

or

$$\bar{\phi} = \bar{\phi}^{+} \left(\frac{U_e^{\,2}}{U_o^{\,2}} \right) \tag{A17}$$

In equation (A17) the minus sign has been dropped. It is also noted that $\bar{\phi}^+$ is of opposite sign to $\bar{\phi}$.

The following relations exist between the plate-fixed and the shock-fixed reference frames:

$$\left.\begin{aligned} \bar{x} + \bar{x}^+ &= U_s \bar{t} \\ U_o + U_e &= U_s \end{aligned}\right\} \tag{A18}$$

From equations (A11) and (A17) the following relation is obtained for shock regions after substituting for $\bar{x}^+$ and U_e:

$$\bar{\phi}(\alpha,\beta,\bar{\gamma}) = \left[\frac{\alpha(A-1)^4}{A-\alpha}\right]^{1/5} \frac{M^+(\beta)}{(\alpha\bar{\gamma})^{1/5}} \tag{A19}$$

therefore,

$$\phi(\alpha,\beta) = (\alpha\bar{\gamma})^{1/5}\bar{\phi}(\alpha,\beta,\bar{\gamma}) = \left[\frac{\alpha(A-1)^4}{A-\alpha}\right]^{1/5} M^+(\beta) \tag{A20}$$

For $\alpha = 1$ equation (A20) gives

$$\phi(1,\beta) = (A-1)^{3/5} M^+(\beta) \tag{A21}$$

APPENDIX B

SHOCK PARAMETERS IN AN IDEAL GAS

To be consistent with the rest of the analysis and for the sake of simplicity, the following properties of the gas are assumed:

(1) The ideal equation of state.

(2) c_p = Constant, c_v = Constant.

With these assumptions, the following relations are obtained from reference 17:

$$A = \frac{U_s}{U_o} = \frac{\gamma + 1}{2} \frac{M_s^2}{M_s^2 - 1} \tag{B1}$$

$$\frac{U_o^2}{h_o} = \frac{4(\gamma - 1)}{(\gamma + 1)^2} \frac{T_1}{T_o} \left(M_s - \frac{1}{M_s} \right)^2 \tag{B2}$$

$$\frac{T_o}{T_1} = 1 + \frac{2(\gamma - 1)}{(\gamma + 1)^2} \left[\gamma M_s^2 - \frac{1}{M_s^2} + (1 - \gamma) \right] \tag{B3}$$

where T_1 is the temperature of the gas in front of the shock. The temperature T_1 has been taken as T_w (=300 K) in this analysis. Further,

$$\frac{U_o^2}{h_w} = \frac{U_o^2}{h_o} \frac{h_o}{h_w} = \frac{U_o^2}{h_o} \frac{T_o}{T_1} \tag{B4}$$

since c_p is assumed to be constant and $T_1 = T_w$.

REFERENCES

1. Trimpi, Robert L.: A Preliminary Theoretical Study of the Expansion Tube, a New Device for Producing High-Enthalpy Short-Duration Hypersonic Gas Flows. NASA TR R-133, 1962.

2. Gupta, Roop N.: An Analysis of the Relaxation of Laminar Boundary Layer on a Flat Plate After Passage of an Interface With Application to Expansion-Tube Flows. NASA TR R-397, 1972.

3. Gupta, Roop N; and Trimpi, Robert L.: Relaxation of the Accelerating-Gas Boundary Layer to the Test-Gas Boundary Layer on a Flat Plate in an Expansion Tube. Recent Developments in Shock Tube Research, Daniel Bershader and Wayland Griffith, eds., Stanford Univ. Press, 1973, pp. 449-461.

4. Bushnell, Dennis M.; and Beckwith, Ivan E.: Calculation of Nonequilibrium Hypersonic Turbulent Boundary Layers and Comparisons With Experimental Data. AIAA J., vol. 8, Aug. 1970, pp. 1462-1469.

5. Mirels, Harold: Boundary Layer Behind Shock or Thin Expansion Wave Moving Into Stationary Fluid. NACA TN 3712, 1956.

6. Trimpi, Robert L.; and Cohen, Nathaniel B.: A Nonlinear Theory for Predicting the Effects of Unsteady Laminar, Turbulent, or Transitional Boundary Layers on the Attenuation of Shock Waves in a Shock Tube With Experimental Comparison. NASA TR R-85, 1961. (Supersedes NACA TN 4347.)

7. Van Driest, E. R.: Turbulent Boundary Layer in Compressible Fluids. J. Aeronaut. Sci., vol. 18, no. 3, Mar. 1951, pp. 145-160, 216.

8. Lam, Sau-Hai: Shock Induced Unsteady Laminar Compressible Boundary Layers on a Semi-Infinite Flat Plate. Ph. D. Thesis, Princeton Univ., 1958.

9. Harris, Julius E.: Numerical Solution of the Equations for Compressible Laminar, Transitional, and Turbulent Boundary Layers and Comparisons With Experimental Data. NASA TR R-368, 1971.

10. Meier, H. U.; and Rotta, J. C.: Experimental and Theoretical Investigations of Temperature Distributions in Supersonic Boundary Layers. AIAA Paper No. 70-744, June-July 1970.

11. Trimpi, Robert L : A Theoretical Investigation of Simulation in Expansion Tubes and Tunnels. NASA TR R-243, 1966.

12. Ames, William F.: Numerical Methods for Partial Differential Equations. Barnes & Noble, Inc., c.1969.

13. Moore, D. R.; and Harkness, J.: Experimental Investigation of the Compressible Turbulent Boundary Layer at Very High Reynolds Numbers, M = 2.8. Rep. No. 0-71000/4R-9, LTV Res. Center, Apr. 1964.

14. Spalding, D. B.; and Chi, S. W.: The Drag of a Compressible Turbulent Boundary Layer on a Smooth Flat Plate With and Without Heat Transfer. J. Fluid Mech., vol. 18, pt. 1, Jan. 1964, pp. 117-143.

15. Schlichting, Hermann (J. Kestin, transl.): Boundary-Layer Theory. Sixth ed., McGraw-Hill Book Co., Inc., 1968, p. 604.

16. Cook, William J.: Prediction and Measurement of Heat Transfer Rates for the Shock-Induced Unsteady Laminar Boundary Layer on a Flat Plate. NASA CR-114582, 1972.

17. Gaydon, A. G.; and Hurle, I. R.: The Shock Tube in High-Temperature Chemical Physics. Reinhold Pub. Corp., 1963.

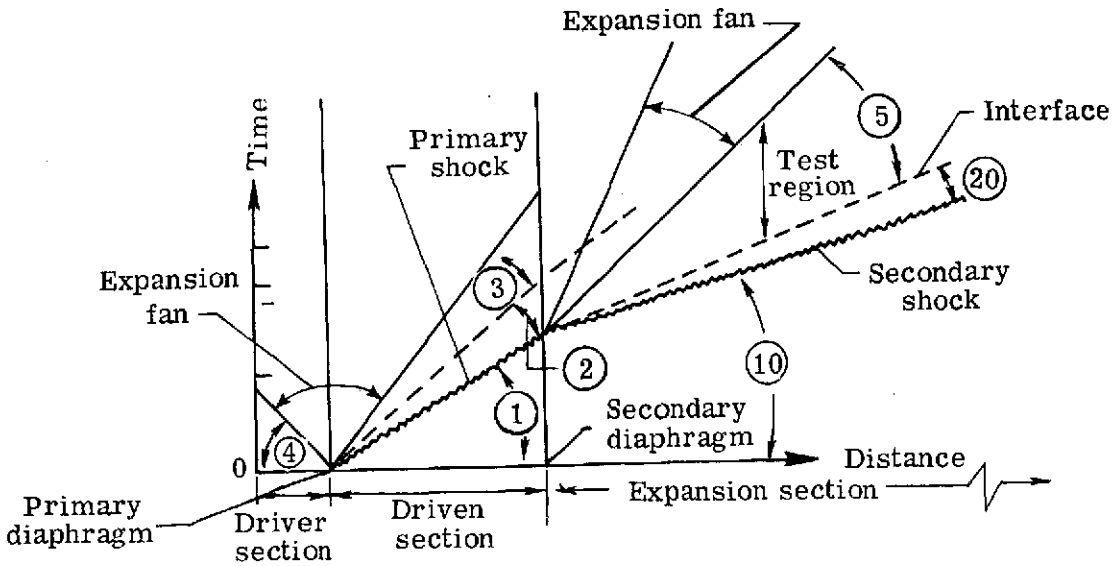

Figure 1.- Distance-time plot of expansion-tube flow. (Taken from ref. 1; circled numbers are explained therein.)

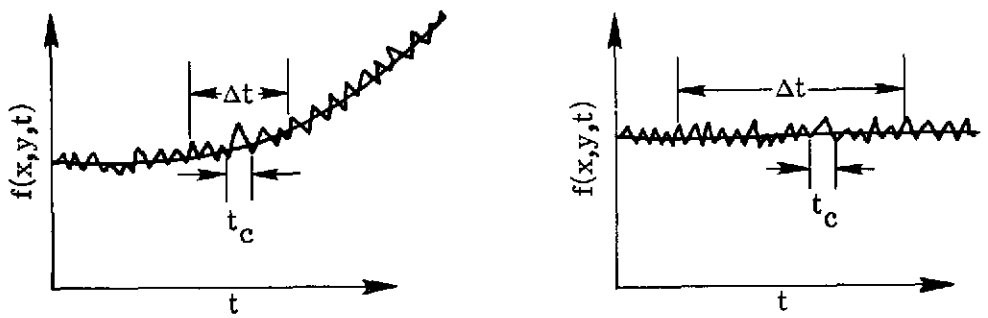

(a) Time-dependent mean flow. (b) Time-steady mean flow.

Figure 2.- Schematic diagram showing time-averaging method employed. (Δt, averaging interval; t_c, characteristic fluctuation period.)

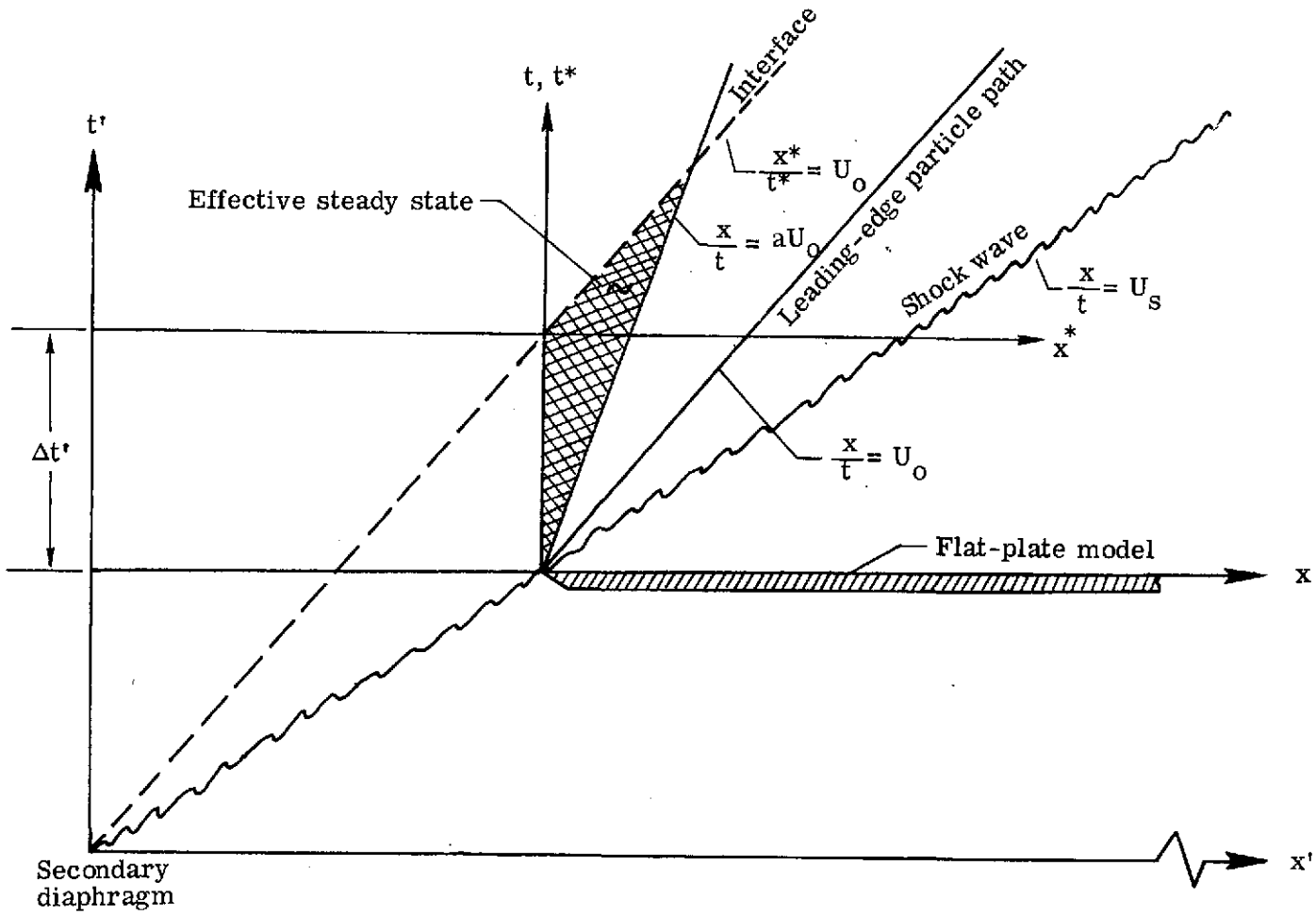

(a) Distance-time diagram for BL limit.

Figure 3.- Schematic representation of BL limit.

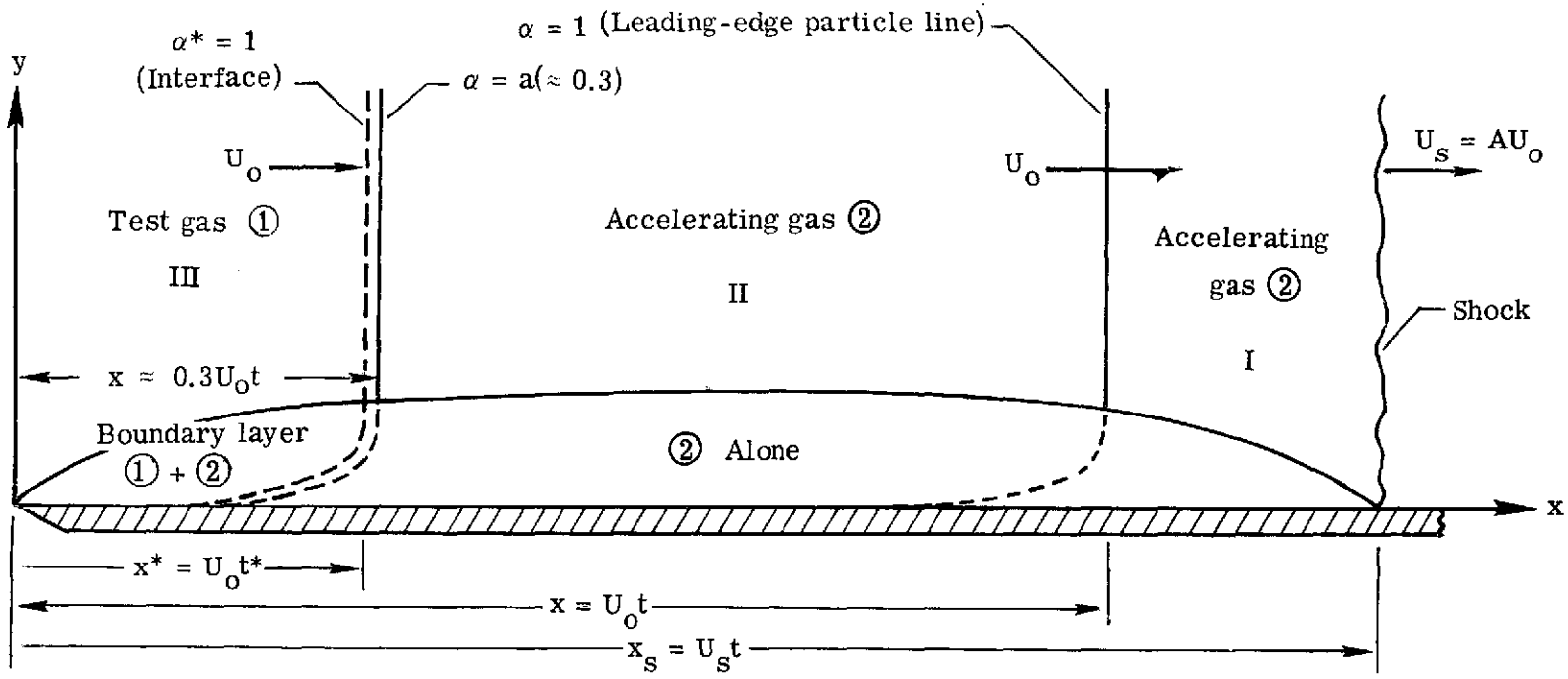

(b) Schematic representation of flow field in BL limit (physical plane).

Figure 3.- Concluded.

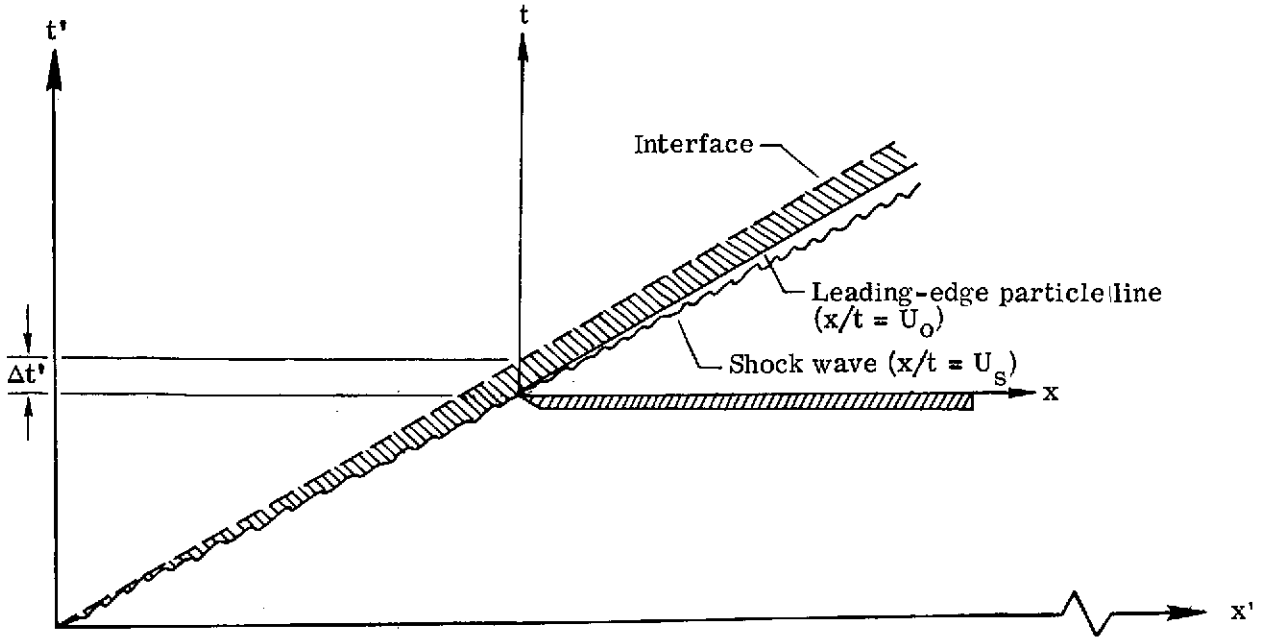

(a) Distance-time diagram for MR limit.

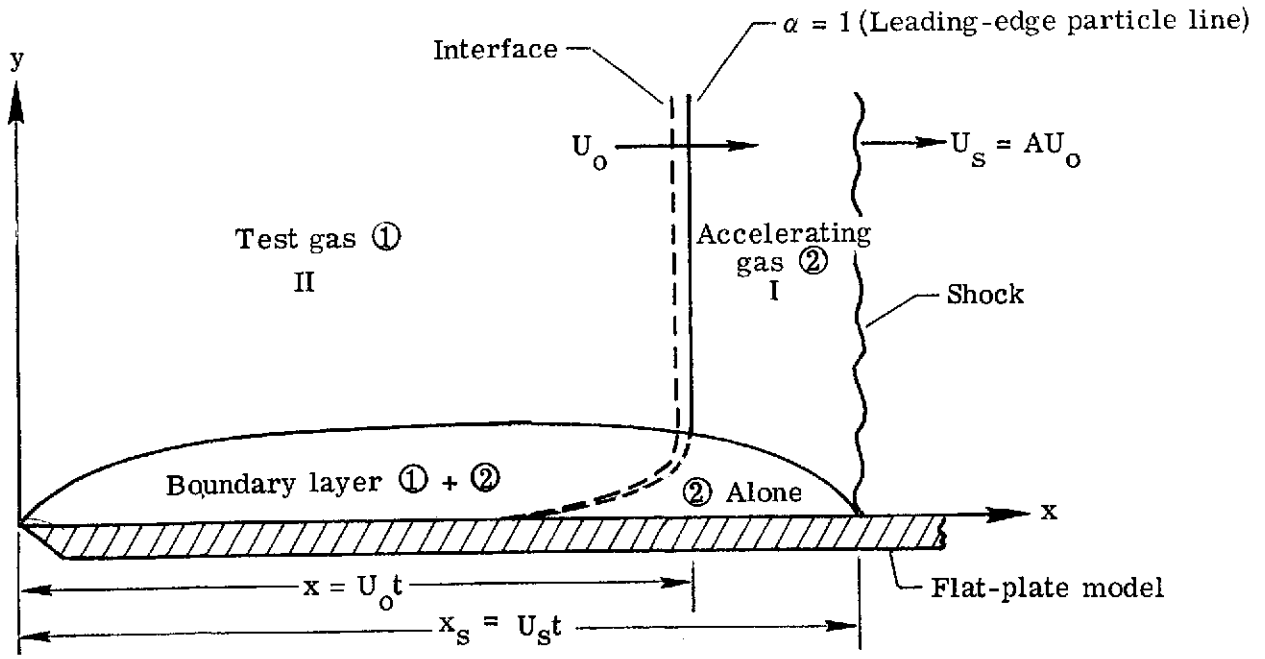

(b) Schematic representation of flow field in MR limit (physical plane). Time delay represented by shaded region is assumed to be vanishingly small.

Figure 4.- Schematic representation of MR limit.

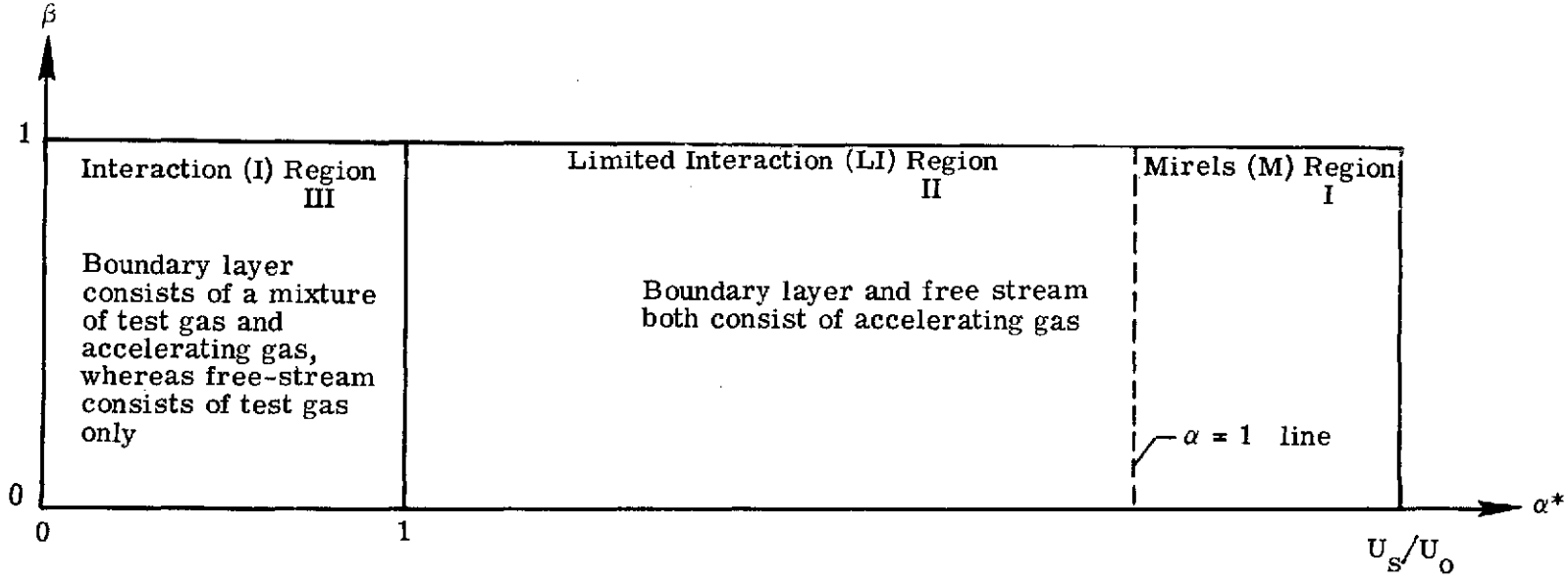

(a) Schematic representation of flow field in α^*, β-plane.

Figure 5.- Blasius (or BL) limit.

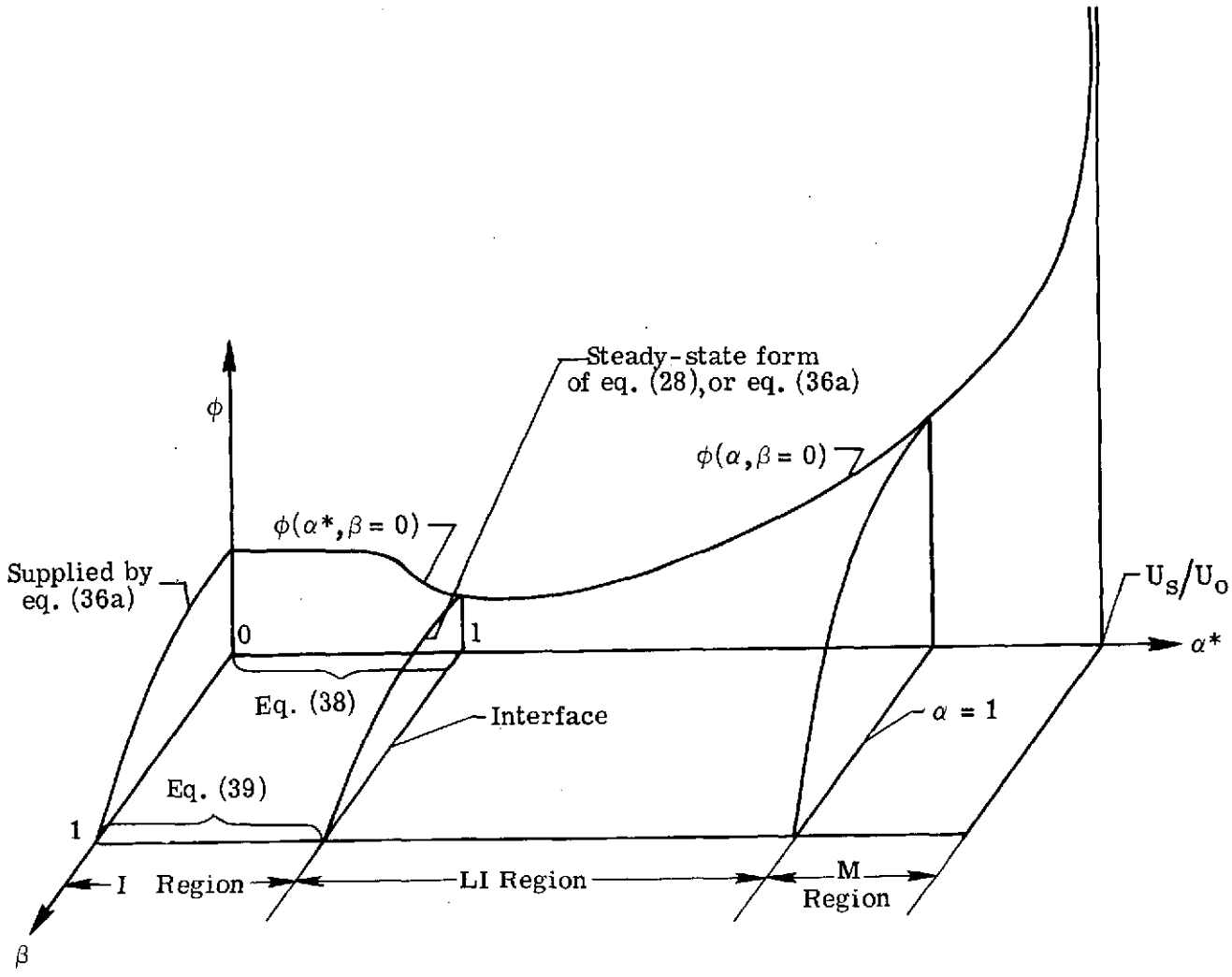

(b) Specification of boundary conditions on ϕ in I region.

Figure 5.- Continued.

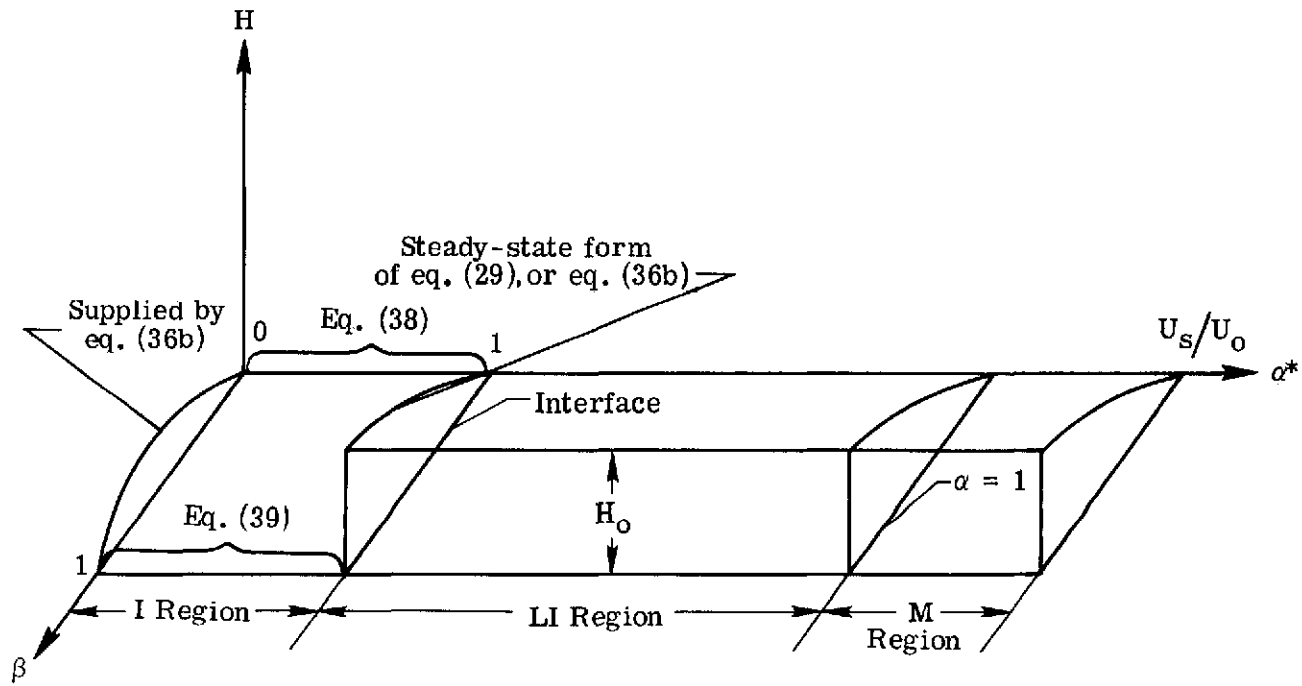

(c) Specification of boundary conditions on H in I region.

Figure 5.- Concluded.

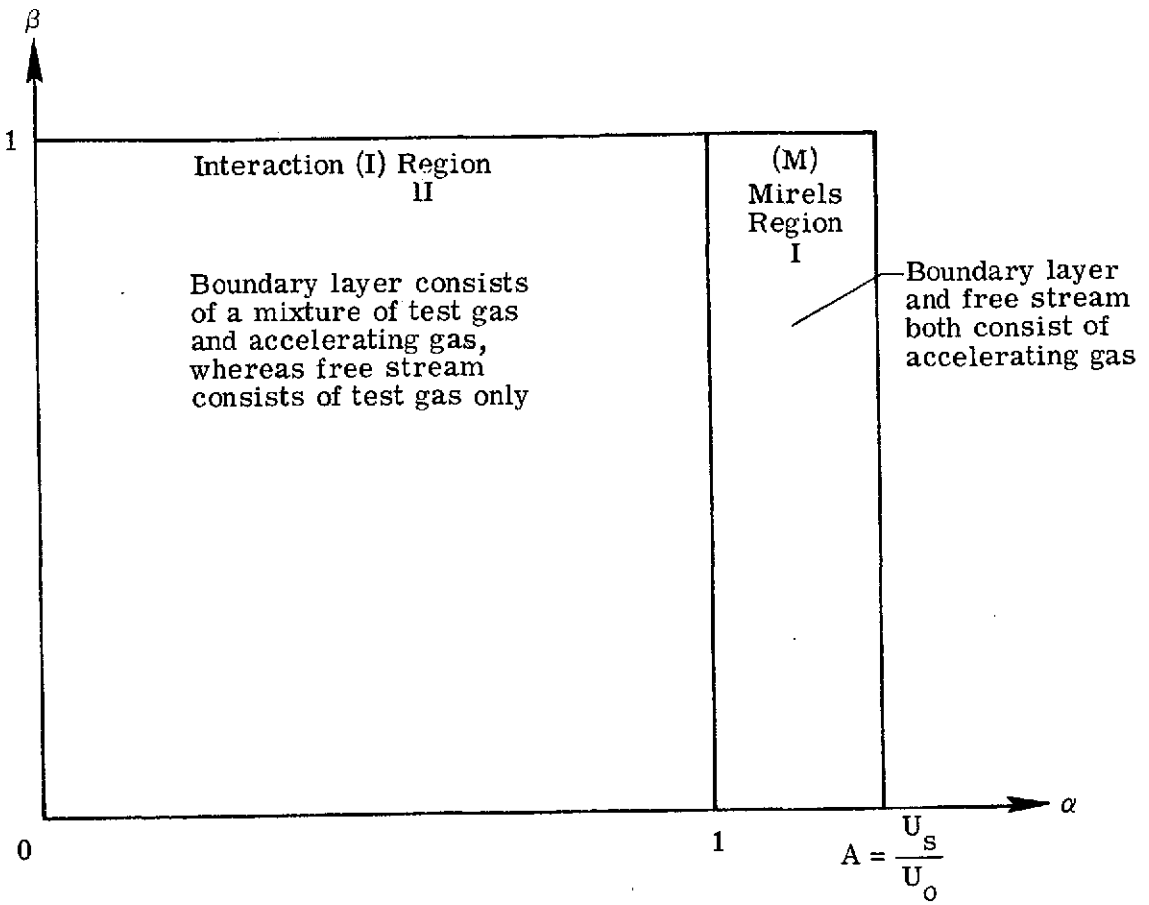

(a) Schematic representation of flow field in α, β-plane.

Figure 6.- Mirels (or MR) limit.

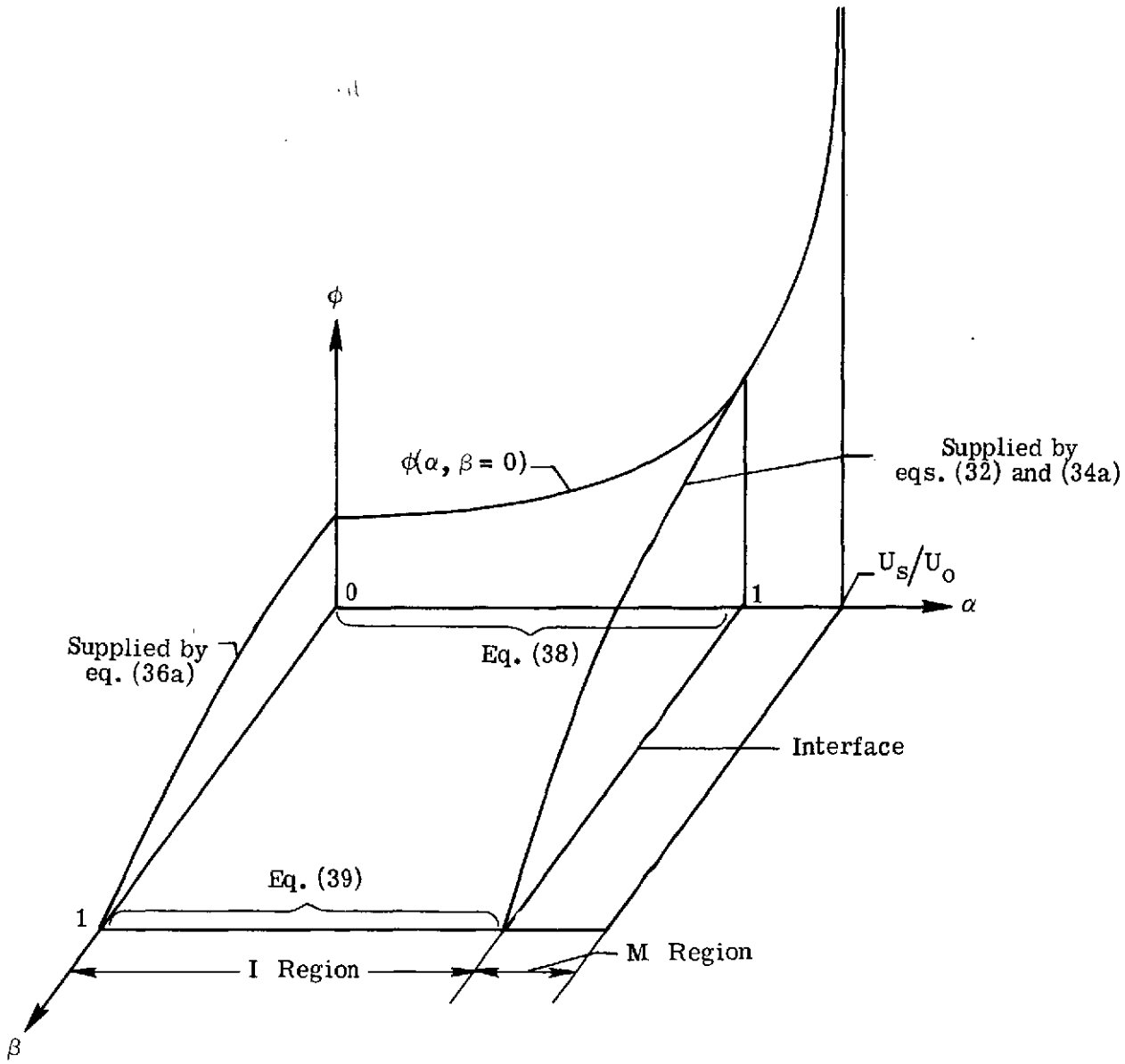

(b) Specification of boundary conditions on ϕ in I region.

Figure 6.- Continued.

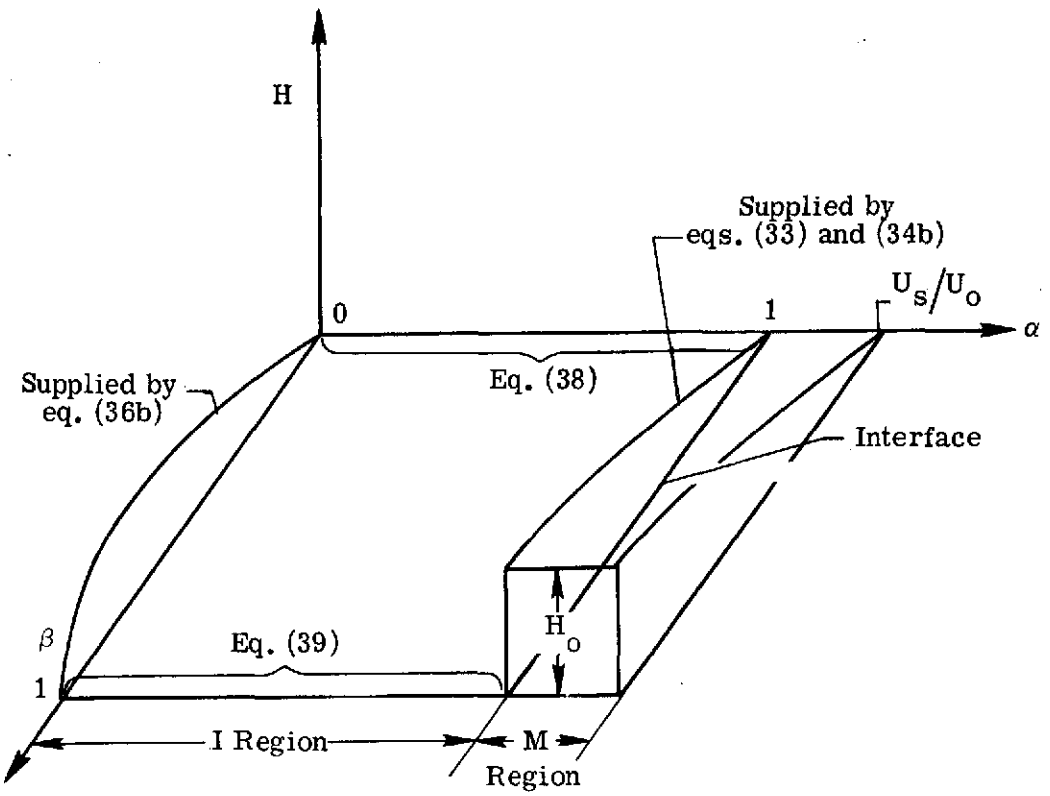

(c) Specification of boundary condition on H in I region.

Figure 6.- Concluded.

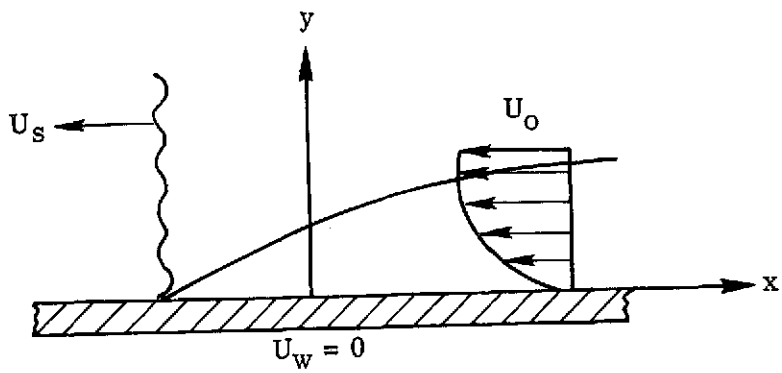

(a) Plate-fixed coordinate system.

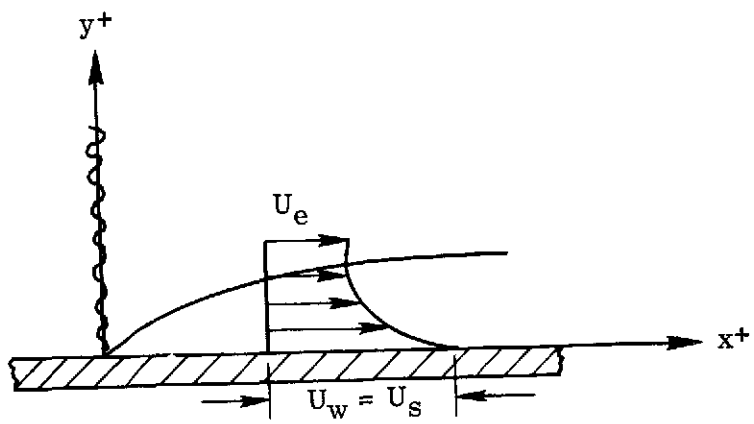

(b) Shock-fixed coordinate system.

Figure 7.- Shock-region boundary layers.

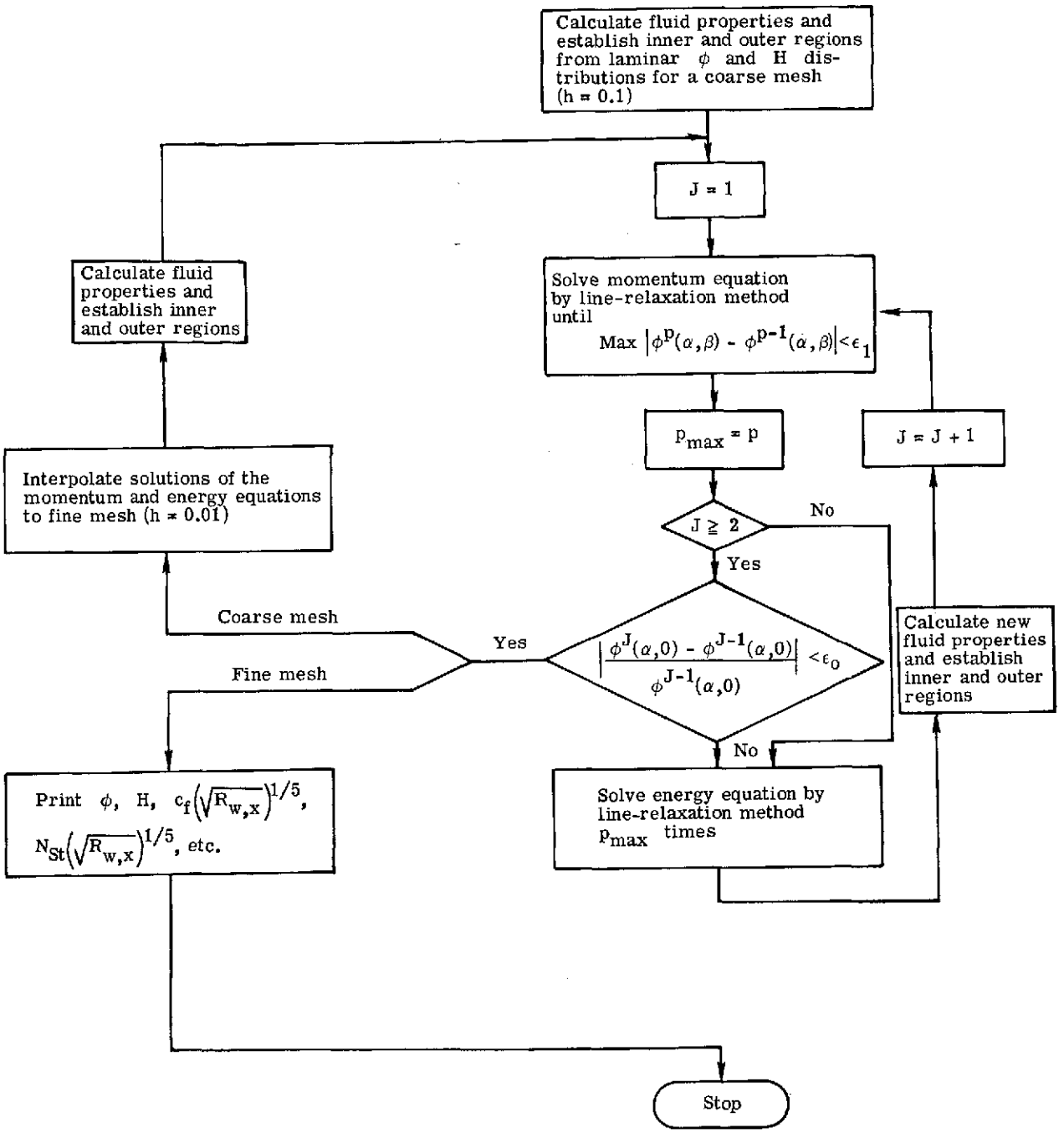

Figure 8.- Flow-diagram for solving turbulent boundary-layer equations.

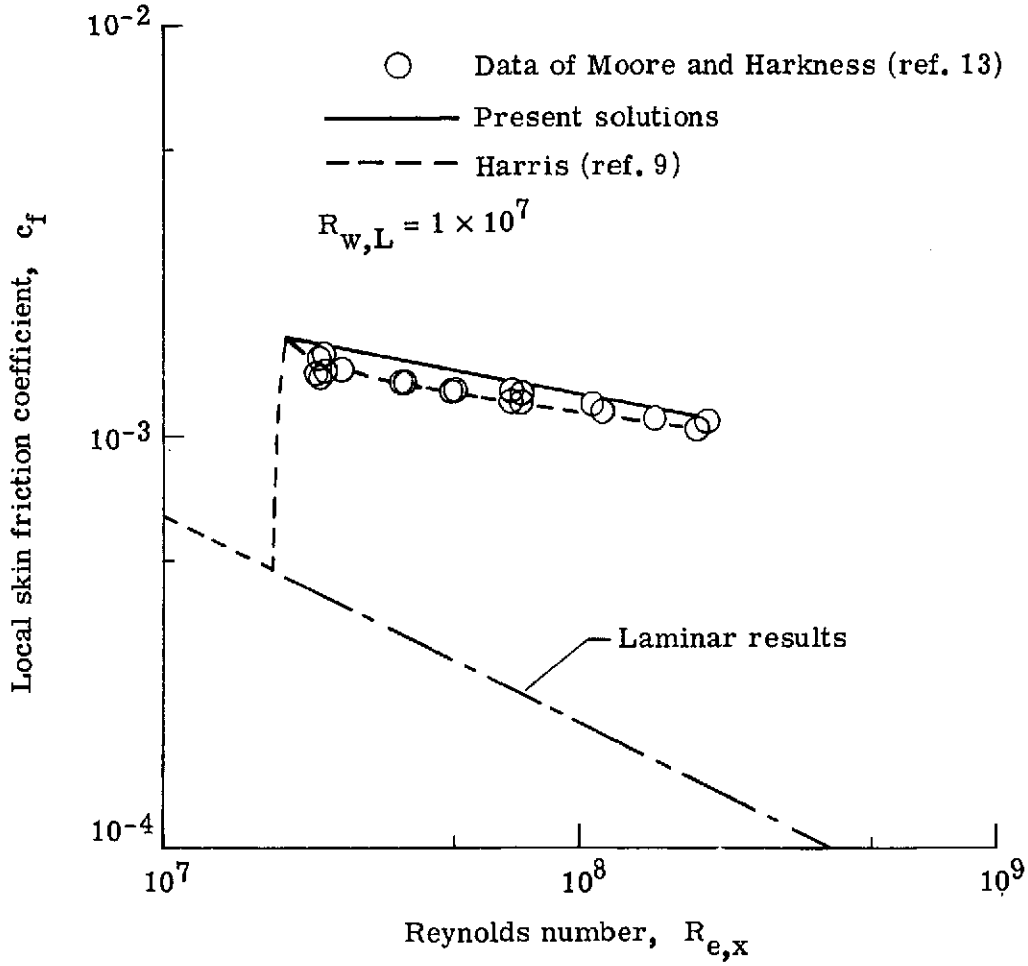

Figure 9.- Variation of local skin-friction coefficient with Reynolds number.

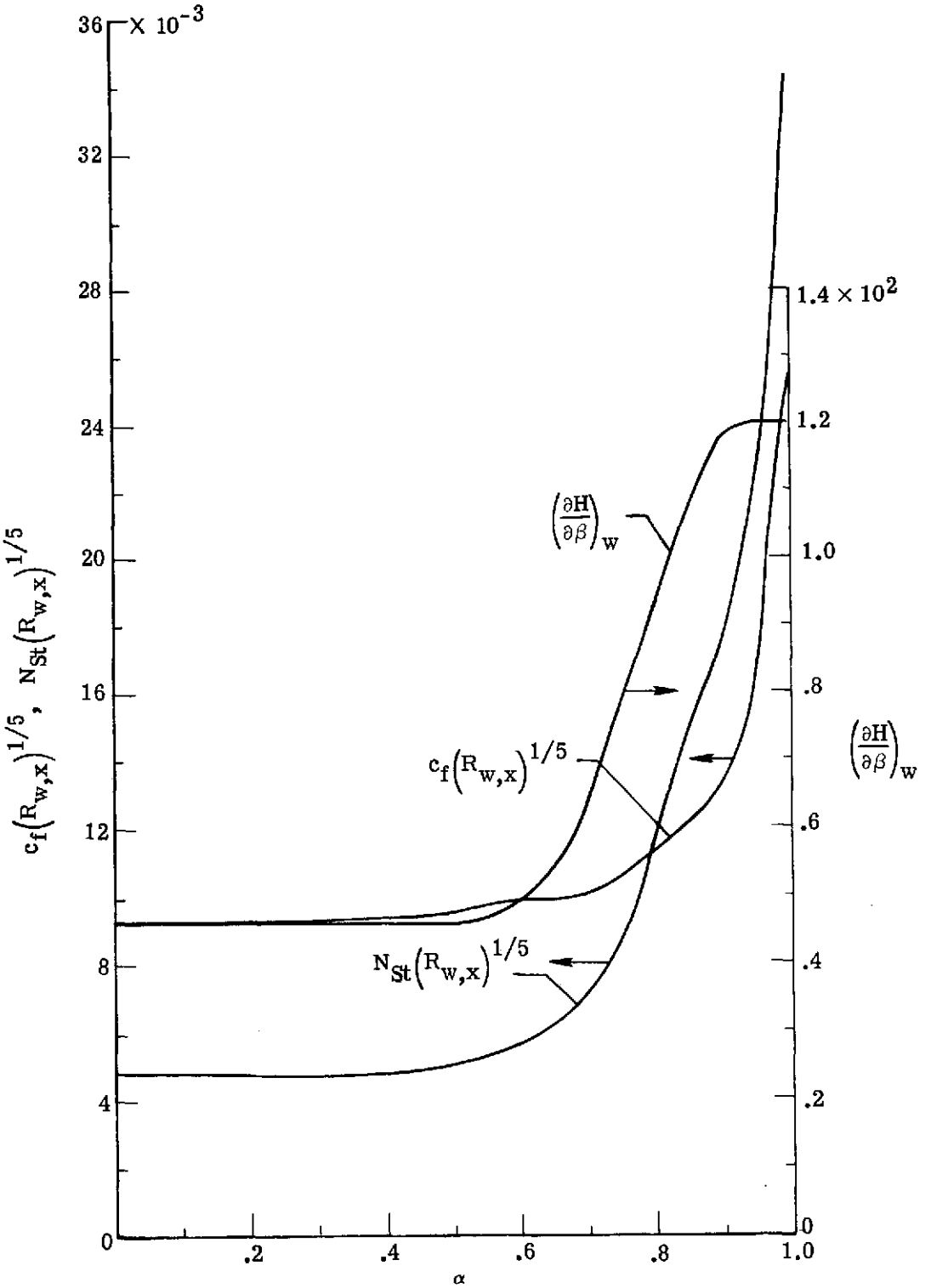

Figure 10.- Distributions of local skin-friction coefficient, Stanton number and gradient of dimensionless local enthalpy; MR limit.

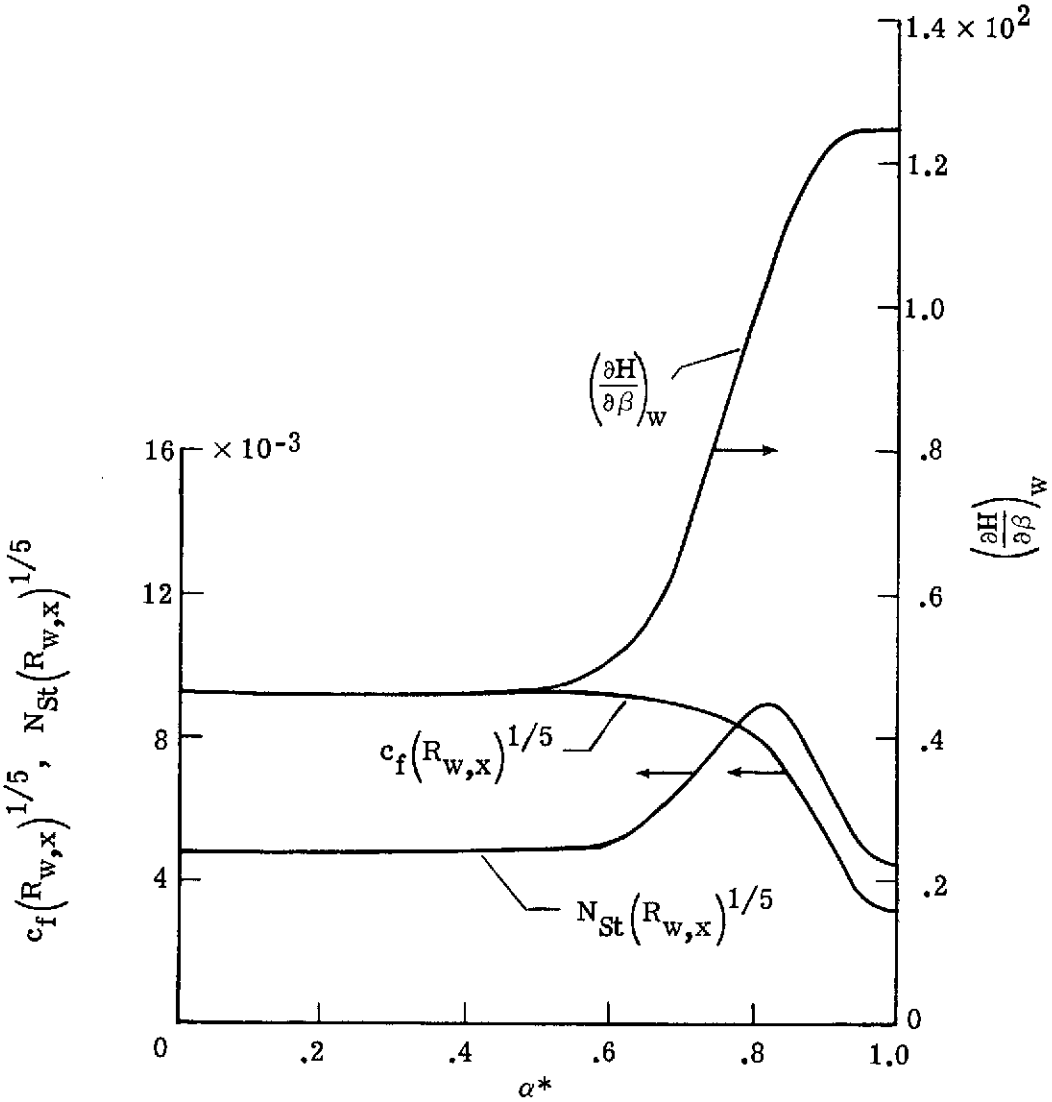

Figure 11.- Distributions of local skin-friction coefficient, Stanton number, and gradient of dimensionless local enthalpy; BL limit.

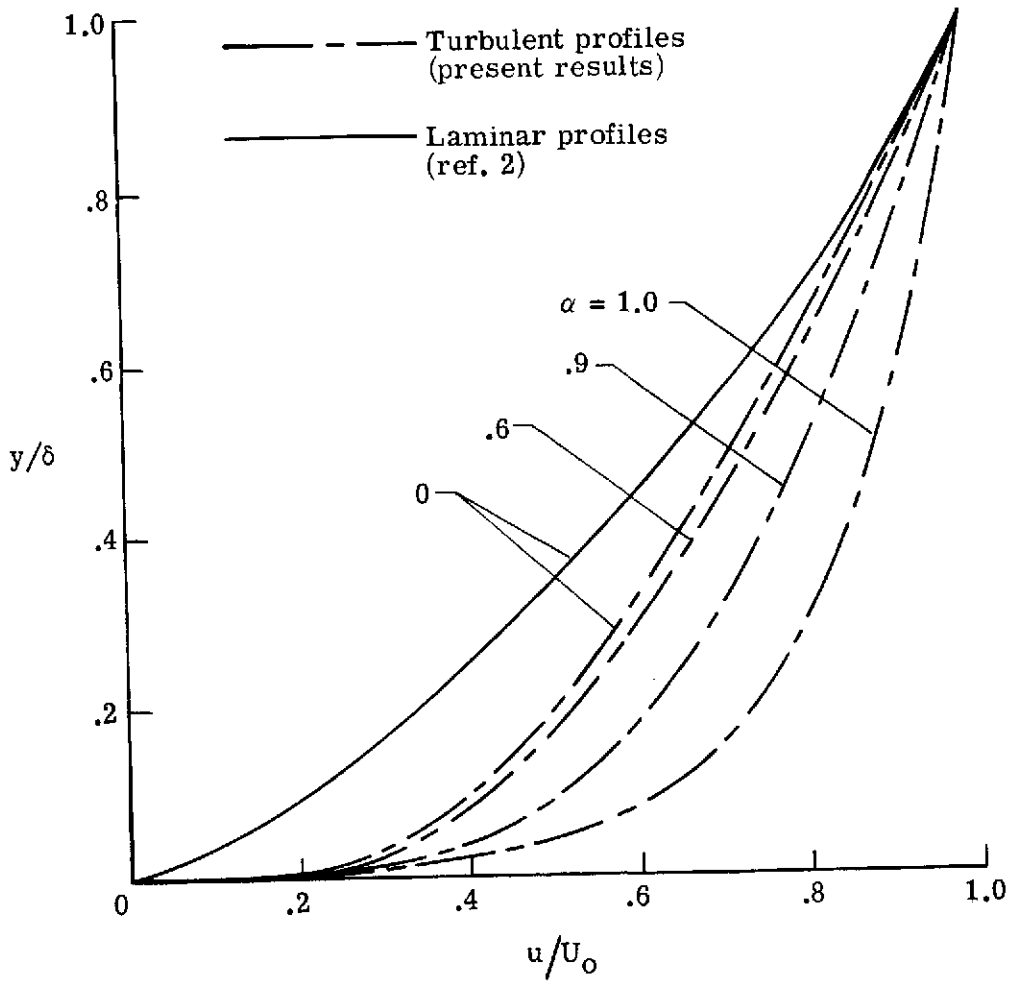

Figure 12.- Velocity distribution through boundary layer for $M_s = 20.8$ in nitrogen; MR limit.

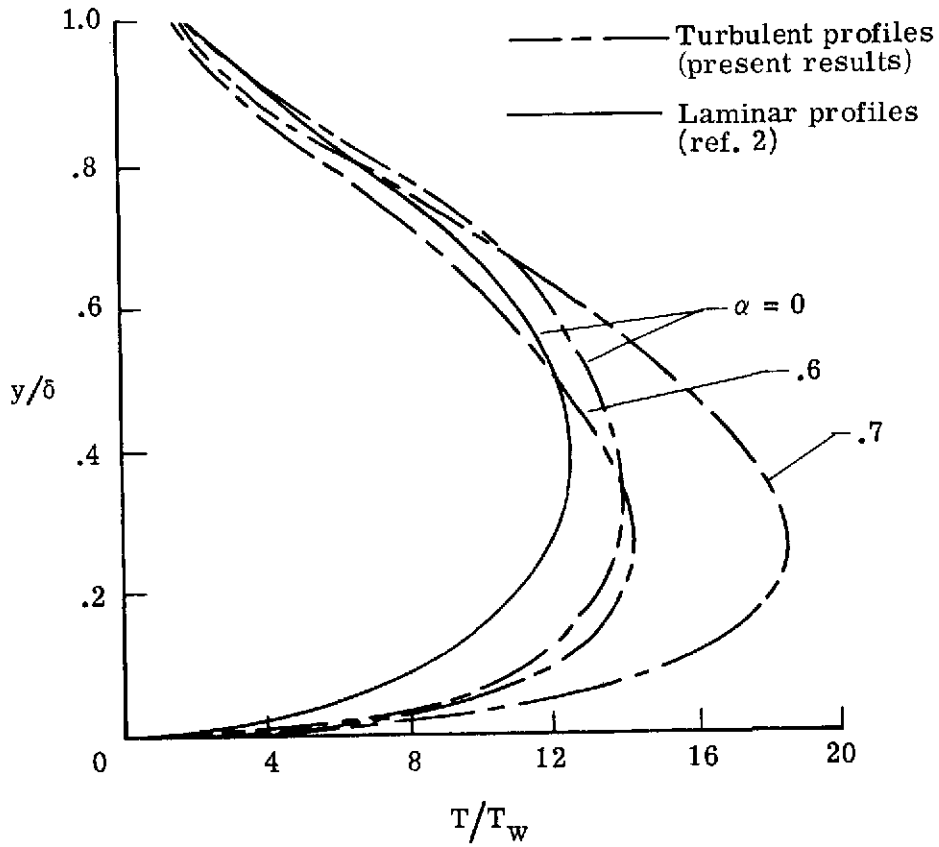

Figure 13.- Temperature distribution through boundary layer for $M_S = 20.8$ in nitrogen; MR limit.

NASA-Langley, 1974 L-9168